

SIMULATION AND OPTIMIZATION OF
AN ETHYLENE PLANT

by

MEISONG YAN, B.E.

A THESIS

IN

CHEMICAL ENGINEERING


Submitted to the Graduate Faculty
of Texas Tech University in
Partial Fulfillment of
the Requirements for
the Degree of

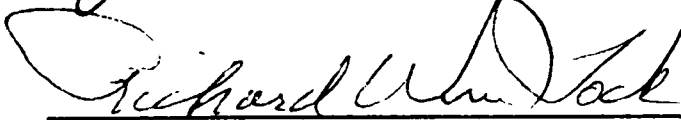
MASTER OF SCIENCE


IN

CHEMICAL ENGINEERING

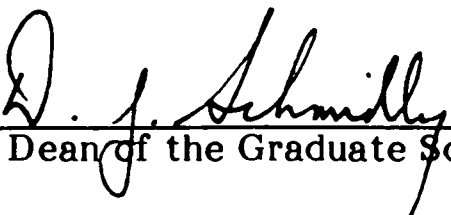
Approved


Chairperson of the Committee





Accepted


Dean of the Graduate School

May, 2000

ACKNOWLEDGMENTS

As the first graduate student to start this project in the Chemical Engineering Department at Texas Tech University, I learned a lot from my research work, not only on the problem solving skills, but also on the importance of the support from my advisor, my professors, my fellow graduate students and my families. Without them, I could not accomplish this task and this thesis would not be possible.

First of all, I would express my sincere thanks to Dr. James B. Riggs for providing me this opportunity to work on this project, and also for his guidance and constant support during the course of this work. He showed me a hardworking mentality and persevering spirit. I will always remember all of his effort in helping me to accomplish this research work.

I also would extend my sincere thanks to Dr. Tock and Dr. Wiesner. I am honored to have two of the best professors in the department as my graduation committee members. What they taught me is far more than my course work. Their patience in replying to my questions enhanced my confidence, and their different research fields broadened my horizon. Most important of all, their optimistic attitude showed me how to survive in the United States. I will not forget all the other professors who helped me to overcome my language barrier and encouraged me to enjoy my life here.

Cordial thanks also should be given to Mr. Rick Dudeck for his help to collect part of the price data in my optimization study, and four engineers working in the chemical industry, Mr. Mark Marinar, Mr. Bob Frisbie, Mr. James Martin and Mr. Scott Rogers. They opened an industrial world for me. In addition to their daily working duty,

they granted me a visit to the ethylene plant, showing me how to collect data from the Engineer Work Station. And I would especially like to thank Jim; he answered all my process questions as quickly as possible by e-mail and by phone without a complaint.

My special thanks go to my fellow graduate students. We discussed problems together; we worked together for the consortium meeting. We laughed when we made progress; we helped each other when we had troubles. We really worked together like a big family. They are Andrei, Marshall, Satish, Govind, Kishor, Xuan, Haitao, Rodney, Scott, Joe, Mat, Sai, Krishna, Arland ... Govind's deep industrial experience broadened my idea about my research, while Guangpu Jin, one of my Chinese friends, showed me the mechanical engineering aspect in my modeling work. I am so lucky to study and work with these nice colleagues, and I am hoping to have an opportunity to work with them again some day.

In the end, I would like to say that all of my achievement could not be possible without my parents' support and my brothers' encouragement. I dedicate my thesis to them.

TABLE OF CONTENTS

ACKNOWLEDGEMENTS.....	ii
ABSTRACT.....	vii
LIST OF TABLES.....	viii
LIST OF FIGURES.....	x
CHAPTER	
1. INTRODUCTION.....	1
1.1 Physical Properties and Industrial Usage of Ethylene.....	1
1.2 Other By-products in an Ethylene Plant.....	2
1.3 Ethylene Plant Diagram.....	2
1.4 Ethylene Plant in USA.....	4
1.5 Thesis Organization.....	5
2. LITERATURE SURVEY.....	6
3. PROCESS MODELING	11
3.1 Cracking Section.....	14
3.1.1 Chain Reaction Mechanism.....	14
3.1.2 Plug Flow Reactor Model.....	17
3.1.3 Pressure Distribution Calculation.....	19
3.1.4 Coke Formation Model.....	24
3.1.5 Heat Transfer Correlation.....	27
3.1.6 Furnace Simulation and Benchmark Result.....	31
3.2 Quench Section.....	39
3.2.1 Quench Process and Waste Heat Recovery.....	39

3.2.2	Tar Condensation.....	40
3.3	Separation Section.....	41
3.3.1	Distillation Technology.....	41
3.3.2	Separation System General Design.....	42
3.3.3	Characteristics of Each Unit.....	44
3.3.4	Approximate Model Approach.....	46
3.3.5	Refrigeration System Model.....	53
3.3.6	Refrigeration System in an Ethylene Plant.....	54
3.3.7	Benchmark Result.....	59
4.	OPTIMIZATION APPROACH.....	61
4.1	Chemical Industry Optimization.....	61
4.2	Mathematical Formulate.....	63
4.3	NPSOL Package.....	64
5.	OPTIMIZATION STUDY.....	66
5.1	Characteristic of the Optimization Study.....	66
5.2	Results of the Optimization Analysis.....	73
6.	DISCUSSION, CONCLUSION AND RECOMMENDATIONS.....	77
6.1	Summary.....	77
6.2	Recommendations.....	78
	BIBLIOGRAPHY.....	82
	APPENDIX	85
A.	THE REACTION NETWORK FOR E/P FEED.....	85

B. VISCOSITY OF GAS MIXTURE AT LOW PRESSURE.....	93
C. REACTION HEAT CALCULATION.....	95
D. ENTHALPY CALCULATION BY SRK STATE EQUATION.....	96
E. PHYSICAL PROPERTIES DATA.....	98

ABSTRACT

The objective of this project is to develop a simplified ethylene plant model, which includes a thermal cracking section, a separation system and an integrated refrigeration system, and use it to study plant-wide time-domain optimization.

The mixture of ethane and propane is feedstock for the cracking furnace while free radical mechanism is a basis for the decomposition of hydrocarbons. A one-dimensional plug flow model, integrated by LSODE package, is employed to describe the species profile, temperature profile, pressure profile, and coke thickness profile, and benchmarked by the industrial data. The pyrolysis gas is sent to a series of distillation for separations into the final products. An approximate model with lumping technology is used to predict the top and bottom product impurity and the required refrigerant, which are also benchmarked by plant data.

NPSOL is used to search the optimal operation points for the processes. Because of the simplification in the modeling work, preliminary optimization results are obtained. The optimization results show that the furnace part is the heart of the ethylene plant while the separation system and refrigeration system limits the maximum furnace effluent. By adjusting the feedstock flow rate and the dilution steam to hydrocarbon ratio, the gross profit of the plant is increased by 6%, comparing to the base case data.

E.2. Heat capacity constants for molecular species	101
E.3. Heat capacity for free radicals.....	102
E.4. State-equation parameters for components.....	103

LIST OF TABLES

3.1. Kinetic data for coke formation model.....	26
3.2. The empirical constants for the thermal conductivity.....	30
3.3. Furnace benchmark results.....	32
3.4. General separation system design data.....	49
3.5. General separation system operation data.....	50
3.6. General separation system feed condition.....	51
3.7. General separation system operation result.....	52
3.8. Two levels of ethylene refrigerant.....	55
3.9. Four levels of propylene refrigerant.....	55
3.10. Typical ethylene refrigerant compressor operation point.....	58
3.11. Typical propylene refrigerant compressor operation point.....	58
5.1. Price data I (unit: \$/lb).....	70
5.2. Price data II (unit: cent/gallon).....	71
5.3. Specific gravity and the converted price.....	72
5.4. List of decision variables.....	73
5.5. Pyrolysis gas flow rate and its composition (mole%).....	75
5.6. Economic analysis of each final product	75
A.1. Reaction network and its kinetic data.....	86
A.2. Components list and their related reactions.....	91
A.3. Free radicals list and their related reactions.....	92
E.1. Component enthalpy of formation and molecular weight	99

LIST OF FIGURES

1.1. General ethylene plant diagram sheet.....	3
3.1. Simplified schematic process flowsheet of an ethylene plant.....	12
3.2. Process simulation and optimization flowsheet.....	13
3.3. Tube heat transfer diagram.....	30
3.4. Component species distribution along the reactor.....	35
3.5. Free radical species distribution along the reactor.....	35
3.6. Temperature distribution along the reactor.....	36
3.7. Initial pressure distribution versus linear pressure drop assumption.....	36
3.8. Benchmark result for the furnace effluent.....	37
3.9. Ethylene product profile during the entire run.....	37
3.10. Coke thickness Profile during the entire run.....	38
3.11. Pressure Profile during the entire run.....	38
3.12. Tube skin temperature Profile during the entire run.....	39
3.13. Typical separation system design in an ethylene plant.....	43
3.14. Simplest refrigerant cycle in a refrigeration system.....	53
3.15. Typical refrigeration system design in an ethylene plant.....	57
3.16. Heat duty requirement benchmark.....	60
3.17. Refrigerant compressor BHP benchmark.....	60
5.1. Economic comparison between base case and optimization result.....	76
5.2. Flow rate comparison between base case and optimization result.....	76

CHAPTER 1

INTRODUCTION

1.1 Physical Properties and Industrial Usage of Ethylene

Ethylene ($\text{H}_2\text{C}=\text{CH}_2$) is almost the lightest organic product in the earth. It is colorless and flammable with a slightly sweet smell at normal condition, i.e., ambient temperature and one atmosphere.

Ethylene is also one of the most important olefinic hydrocarbons in the petrochemical industry. The importance comes from its highly reactive double bond in its chemical structure. With this double bond, ethylene can be involved in all kinds of reactions – addition, oxidation, polymerization, among many others – to convert to the final product or intermedial product in the petrochemical engineering industry. In addition, ethylene is also a major raw material to produce plastics, textiles, paper, solvents, dyes, food additives, pesticides and pharmaceuticals. So, the ethylene's use can be extended into the packaging, transportation, construction, surfactants, paints and coatings and other industries.

Ethylene is usually transported by pipeline in gaseous form from the producing plant to the purchasing plant, although a relatively small quantity of liquefied ethylene is moved by tank truck. In the United States, Texas and Louisiana are the major ethylene producing and consuming areas and numerous pipeline networks are constructed to transport gaseous ethylene.

1.2 Other By-products in an Ethylene Plant

Although ethylene is considered to be the major product from an olefins plant, the by-products are also of great importance when considering the plant-wide economics. In the mid-1950s, the by-products of propylene and C_4 's were generally burned with the residue gas as fuel gas and the pyrolysis gasoline was blended into a large gasoline pool without hydrotreating. In the early 1960s, people gradually realized the importance of those by-products and made profit from them. The propylene can be used to produce polypropylene, isopropanol, acrylonitrile and cumene. The pyrolysis gasoline needs hydrotreating before the blending into a gasoline pool. Currently, many plants control the propylene/ethylene weight ratio in a certain range to satisfy the demand for propylene. BASF and Fina (Chang, 1998) even have planned to use olefin metathesis, which can enhance the reactions between n-butenes and ethylene and increase the yield of propylene.

1.3 The Ethylene Plant Diagram

The modern ethylene plant usually has a yield of billions of pounds per year. The majority of the processes are thermal pyrolysis of hydrocarbons, which is mixed with dilution steam. There are also other processes to produce it, like refinery off-gas stream, ethanol dehydration and from coal and coal-based liquids. Some research and investment have been launched on catalytic cracking on hydrocarbons.

Figure 1.1 shows a general process design of an ethylene plant while the detail discussion of thermal cracking is presented in Chapter 3.

The whole process works in this way. The feedstocks, mixed with dilution steam, enters the cracking section and is pyrolysed by heat into small components. The pyrolysis gas enters the quench section and is cooled there to some controlled temperature. Finally, the pyrolysis gas goes into the separation section to be separated into a variety of desired final products. Water enters the water quench tower, a part of quench section, cooling down the high temperature pyrolysis gas and becoming steam. That steam, called dilution steam, mixes with the feedstock before entering the pyrolysis section to decrease the partial pressure of the cracked gases and slow coke formation.

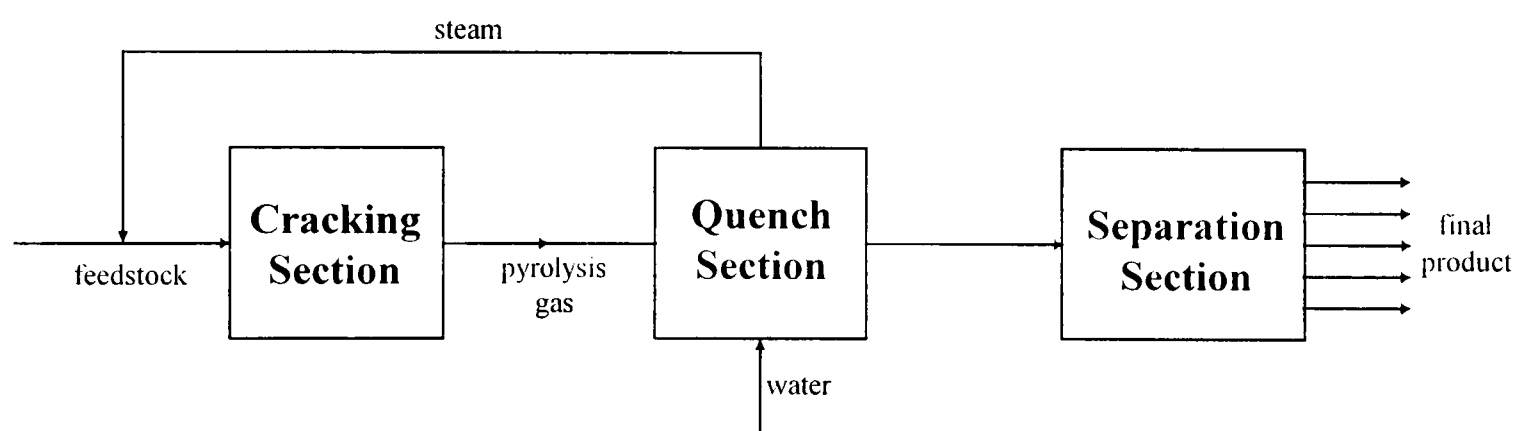


Figure 1.1. A simplified ethylene plant diagram sheet.

A variety of feedstocks can be used in a thermal cracking process. The feedstock for an ethylene plant could be methane, ethane, propane and heavier paraffins. With the development of cracking technology, it can also be cracked from crude oil fractions: naphtha, kerosene and gas oil. Sometimes, raffinates from aromatics extraction facilities can also be used as feedstocks. The choice of feedstock is a compromise of availability, price and yield. This is particularly true in Europe, where many plants combined their oil

refinery process with ethylene plants in order to make full use of the extra low octane naphtha streams coming from refinery plants.

1.4 Ethylene Plant in USA

In the USA, the initial construction of ethylene plants was based on the abundant light hydrocarbons on the Gulf Coast. With the development of thermal cracking technology, the chemical companies switched to constructing naphtha/gas-oil based ethylene plants to find some margin profit from those cheaper feedstocks if considering there are limited natural sources on Gulf Coast. Since more natural sources were discovered in the Mid-East and more convenient pipeline networks were constructed, light hydrocarbons were still remain as the dominant part of the feedstock supply for ethylene plants. Another reason for choosing light hydrocarbon as feedstock is, ethylene plants based on light hydrocarbons are much simpler and cheaper to build and operate than plants designed to use heavy feedstocks. The plant has to employ much greater control over the composition of the final product once the heavier feedstocks are cracked and more variety of components comes. That is also why we choose E/P feed (a mixture of ethane and propane) to begin our study.

The ethylene-producing industry has seen a dramatic increase in the United States after World War II, from an annual yield of 310 million pounds in 1945 to an estimated 12.5 billion pounds in 1968 by the study of the U.S. Department of Commerce (1986). It was reported by Chang (1998) that the annual yield in USA was about 33 million metric tons in 1998, which occupied about 37% of the world product. With the new construction

projects in Exxon, Chevron and other chemical companies, the ethylene plant capacity in USA could reach 35 million metric tons/year in 2000.

1.5 Thesis Organization

For such high yield plants, even a trace of optimization will create huge profit. That is why we began this project. In April 1999, under the direction of Dr. Riggs, I visited a North American ethylene plant and collected the data from its engineer working station to benchmark my model, which is critical to my optimization study.

In my thesis, a substantial amount of literature are collected and reviewed, which is discussed in Chapter 2. Chapter 3 is about the main process units analysis and the corresponding modeling work. The parameter estimation and benchmark work are also included in Chapter 3. Chapter 4 describes the optimization approach and technology while the optimization results of my research work is presented in Chapter 5. The conclusions and recommendations are summarized in Chapter 6.

CHAPTER 2

LITERATURE REVIEW

Several books are available for the general introduction to the ethylene production. Among them, the book edited by Kniel et al. (1980) is highly recommended, which gives a plant-wide overview for the industry. The content of the chapters includes a presentation of the relevant chemistry, the fundamental unit operations, the storage, shipping and handling, and the other related subjects. At the end of this book, literature of an economic analysis of ethylene plants is presented and the future outlook is predicted.

Beside the plant-wide summary, Albright et al. (1983) focus on the cracking section and collect the most recent results and key aspects on the pyrolysis reactions and processes. Cracking theory and reaction networks ranging from the methane to naphtha and even non-petroleum feedstocks are listed in several chapters. Detailed information about the modeling work and its corresponding advantages are discussed after the process analysis.

Simulation and optimization work for the ethylene plant, especially on the cracking furnace model, is considered to be mature since many pyrolysis yield models have been developed in the last three decades. The furnace model could be a simple empirical model, a molecular model, or even a mechanistic model. The feedstock could be considered to focus on simple hydrocarbons, mixture feed, or heavy crude oil. For the simpler models, the prediction range may not be sufficient for the modern plants since most plants will crack a variety of feedstocks which are based on the market supplies. For more detailed models, the CPU time to find a feasible solution sometimes could be

beyond the plant's time limits. Many rigorous commercial models are available in the software market, but usually they are quite expensive.

SPYRO (Dente et al., 1979) is a commercially available rigorous cracking model for an ethylene plant and is popular because of its completeness and flexibility. Its simulation strategy is based on a well-tested mechanistic model and extended to a rigorous reaction scheme. The integration of species profiles is simplified by the assumption that the rate of disappearance is quasi-proportional to the concentration of the component and which reduces the simulation time. The benchmark results for the model predictions against the industrial data also give excellent agreement and are used extensively for furnace control and optimization work.

Other molecular models also provide reliable predictions over a certain limited range of conditions. Among them, the work of Froment and his co-authors is the most prodigious. Their kinetic data about cracking paraffins and its mixture have been compared with data for a pilot plant (Sundaram et al., 1978). A rigorous model with the coke formation is considered. They also propose simple reaction schemes for the cracking of pure ethane and the cracking of pure propane (Sundaram et al., 1981, 1979). The experimental data are used to verify the proposed kinetic equations for the coke formation data, of which the predicted results are in agreement with the industrial data. In their recent work (Heynderickx et al., 1998), they suggest using an elliptical furnace tube to reduce the coke formation rate where they predict will increase the run length by 40% compared with the traditional circular tube.

For a special E/P feed, which is studied in this thesis, Tsai and Zou (1987) use a free reaction scheme consisting of 18 reactions and 10 components to predict

co-cracking. By using Gear's method for numerical integration and comparing the reactor with experimental data, they find the overall selectivity for co-cracking is better than a single feed of ethane or propane.

The separation system is largely composed of distillation columns. The detailed information about the process history, process theoretical analysis and process modeling technology is thoroughly introduced by Kister (1992). Design technology is also introduced in his book, which contains tray design, packing design and scaleup guidelines.

Short-cut methods are used here for modeling the distillation columns in the separation system. Individual researchers have different interpretations for the short-cut method. Those extended methods, derived by Smoker (1938), Smith and Brinkley (1960), Jafarey et al. (1979), are generally based on the McCabe-Thiele diagram and its assumptions. Jafarey's equation is highlighted in this work because of its power to predict the effect of disturbance on the column separation (Jafarey et al., 1979). Douglas et al. (1979) extend its usage to a multi-component system and show that it predicts results accurately.

For an ethylene plant, the separation system and the refrigeration system are highly integrated. Hurstel et al. (1981) analyze the refrigeration needs for an ethylene plant and conclude that a well-organized refrigeration scheme is very important in reducing the plant energy usage. Colmenares et al. (1989) also use the ethylene plant as an example for the synthesis analysis of cascading the refrigeration system and chemical processes and give optimized operation temperatures for each working unit. By using

their temperature lumping technique, the operating cost of the refrigeration system can be significantly reduced.

Huang and Shao (1994) use a pattern recognition method to choose the key elements in the processes for the ethylene plant optimization. Key factors influencing the objective function are chosen by using feature-selection technique and are used for optimal operation study by applying the Fisher rule and fractional correction rules.

Recent literature shows quite a lot of applications in this field. Several large chemical companies have taken the advantages of Real Time Optimization (RTO) technology. Mobil's RTO (Georgiou et al., 1997) in the ethylene plant was accomplished in April 1994. Another company, Chevron (Gibbons et al., 1990), also applied the RTO method and suggested a simplified approach for calculating the changes in Tube Metal Temperature (TMT). The approach is based on an empirical correlation relating changes in feed rate, steam to hydrocarbon ratio and severity to the changes in TMT. Relationships were developed from historical data and test runs done on the furnaces and were proved to be a very good representation for the RTO. Exxon Chemical Company in Baytown area (Bartusiak et al., 1992) also develops their real-time optimization application at a large ethylene plant by rigorous, open-equation-based models. The whole scheme includes process models, the optimization package and the process control system to implement the optimal results.

In those applications, severity is used as the constraint in the optimization study. Severity and conversion are different concepts in the reaction kinetics. However, the severity is referred as the conversion for the E/P feed or the methane/propylene ratio for heavy hydrocarbon feedstock in the ethylene plant. The maximum severity in the plant

means the maximum ethylene yield with an acceptable run-length time for the furnace, which is decided from the daily operation experience.

The optimization results eventually will be sent to the regulatory or advanced control system in the plant to reach the expected extra profit margin. For Mobil (Georgiou et al., 1997), the optimized operation points are implemented via conventional advanced control systems from Setpoint Inc., Dynamic Matrix Control Corp., and other proprietary controllers. The more reasonable the optimization results are, the more feasible the control work will be. A successful case in a control and optimization project is shown by an ethylene unit in Finland (Sourander et al., 1984), which gains 2% extra yield in its ethylene yield by the control and optimization work on the cracking heaters.

CHAPTER 3

PROCESS MODELING

In a thermal cracking ethylene plant, the feedstocks could be naphtha, n-pentane, n-hexane, LPG (propane/butane), and an off-gas stream, which come from the nearby refinery, or hydrocrackers and benzene plants. The choices of the feedstocks basically depend on feed availability and process economics.

Figure 3.1 shows a simplified schematic process flowsheet of a typical ethylene plant which processes E/P feed. The distillation columns series include a demethanizer (DC_1), an ethylene recovery tower (C_2H_4 Recovery), a deethanizer (DC_2), a C_2 splitter, a primary depropanizer (HP DC_3), a secondary depropanizer (LP DC_3), a C_3 splitter and a debutanizer (DC_4). Each unit in this flowsheet is simulated by a semi-rigorous model, which is simplified, but still accurately represents the main issues in the plant. Ethane and propane from the pyrolysis effluent are recycled. A different plant could have different process arrangements, based on the specific considerations and requirements for that plant.

Figure 3.2 gives the process simulation and optimization flowsheet. In this work, the plant measurement data of the tube outlet temperature is used to justify the actual heat transfer to the tube while the initial pressure drop measurement is used to parameterize the tube roughness for the future pressure drop calculation. A process of trial and error is employed until two values are sufficiently close. After the parameterization of the model, the furnace model begins to calculate the species profile, the temperature profile, the pressure profile, the coke thickness profile and the total run-length. The predicted

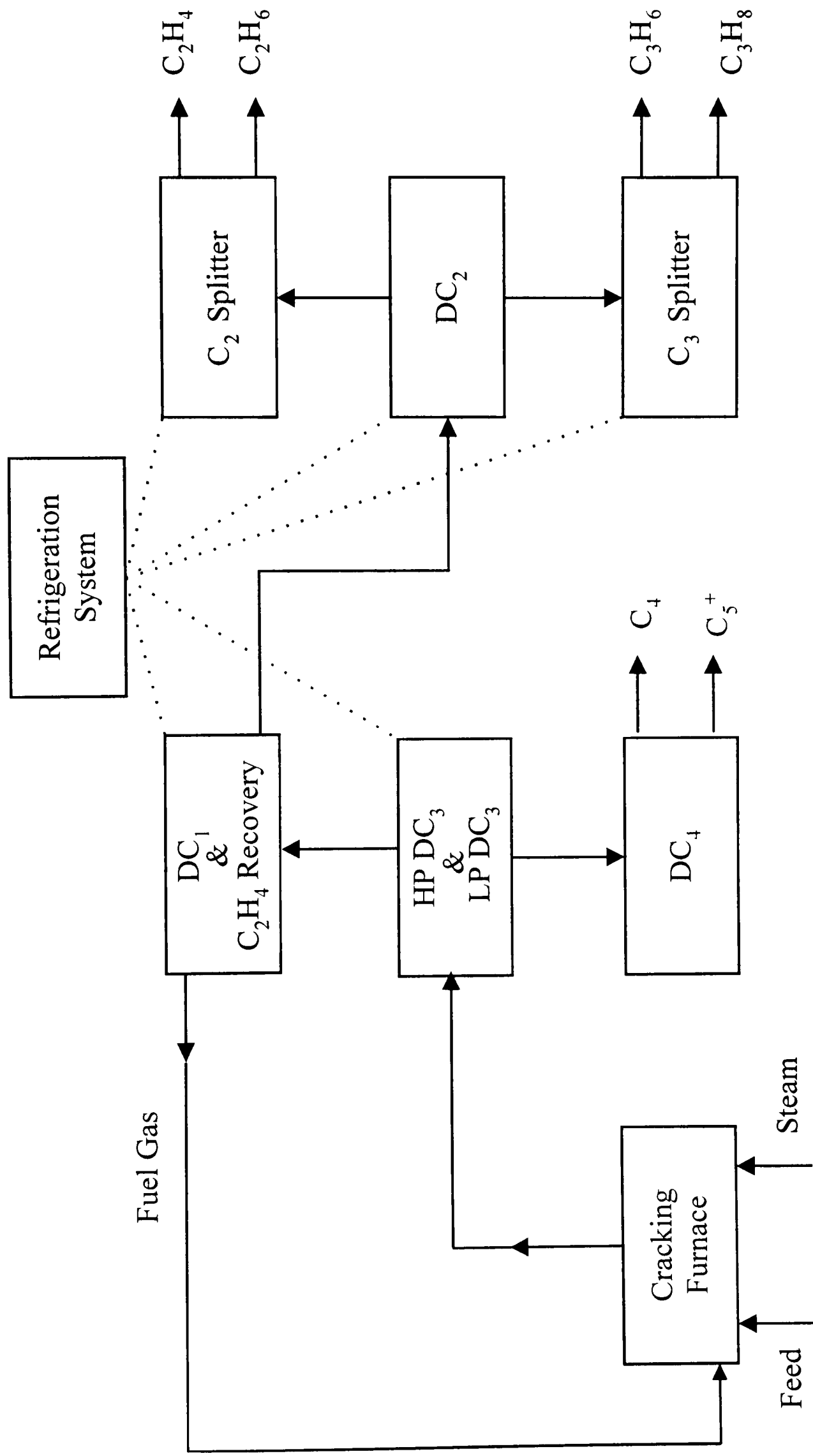


Figure 3.1. Simplified schematic process flowsheet of an ethylene plant.

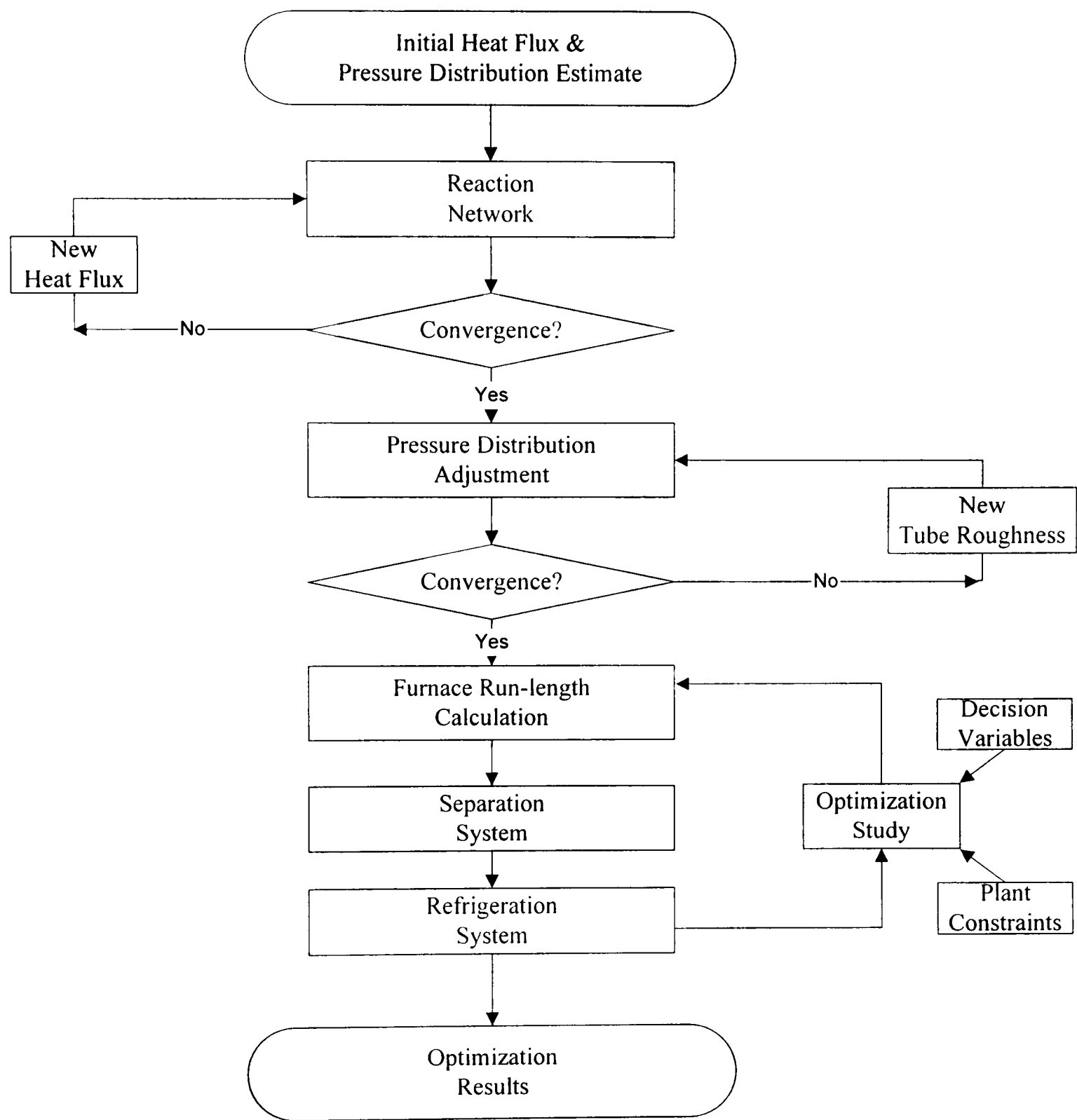


Figure 3.2. Process simulation and optimization flowsheet.

pyrolysis gas flow rate and composition are sent to the model of the separation system to predict the final products. The refrigeration system model is used to calculate utility usage of the separation system. After that, all the modeling results are sent to the optimization package and used for searching an optimized operation region.

3.1 Cracking Section

A thermal cracking furnace is usually divided into two parts: the convection section and the radiant section. The convection section is used for preparation and preheating of the feedstocks. No chemical reactions occur in this section. The radiant section is where the feed is heated rapidly and cracked into ethylene and all other byproducts. All cracking products are sent to the down-stream facilities for separation.

3.1.1 Chain Reaction Mechanism

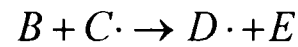
The free radical mechanism is the generally accepted theory for the decomposition of ethane, propane, heavier paraffins and other hydrocarbons. Free radicals are highly reactive molecular fragments containing an unpaired electron. They play a very important part in chemical reactions but exist only for a very short time.

The reaction network includes three consecutive stages: chain initiation, chain propagation and chain termination.

Chain initiation is the stage that creates the intermediate free radicals $M \cdot$ and $N \cdot$ to generate the subsequent reactions



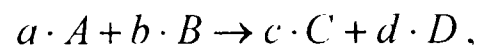
Chain propagation is the stage in which reactions occur between molecular species and free radicals to produce other intermediates $D\cdot$.



Chain termination is the stage that causes the disappearance the free radicals and forms another stable product.



For each reaction, the elementary reaction rate is assumed to be valid. The order of the reaction depends on the molecularity of the species. That is, for a reaction:



the elementary reaction rate will be:

$$r = K \cdot C_A^a \cdot C_B^b \quad (3.1)$$

where

C_A = concentration of species A, mole/liter

C_B = concentration of species B, mole/liter

a = stoichiometric coefficient of species A in the reaction

b = stoichiometric coefficient of species B in the reaction

K = specific reaction rate constant

r = reaction rate, $\text{mole/liter} \cdot \text{sec}$.

Arrhenius equation is used to calculate the dependence of reaction rate constant on the temperature.

$$K(T) = A \cdot e^{-\frac{E}{R \cdot T}} \quad (3.2)$$

where

A = preexponential factor or frequency factor

E = activation energy, kcal/mole

R = gas constant

T = absolute temperature, K .

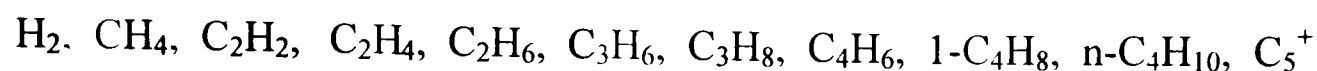
The unit of the frequency factor, which depends on the order of the reaction, could be

sec^{-1} or $\text{L}/\text{mole} \cdot \text{sec}$ in this reaction network.

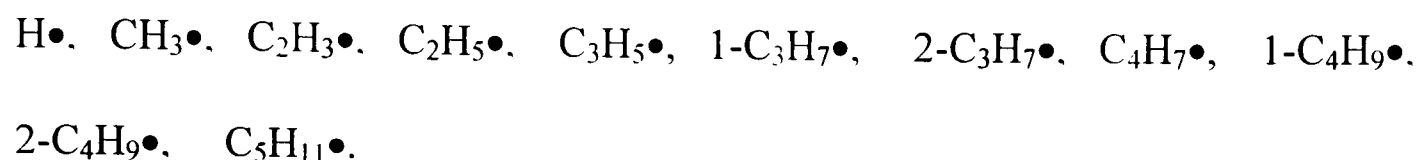
Numerous studies have been done to determine the kinetic values of the activation energy and the frequency factor. Among them, the kinetic data published by Froment and his co-authors are the most accepted ones. They established a set of experiments to determine the kinetic approach for both ethane cracking model (Sundaram et al., 1981) and propane cracking model (Sundaram et al., 1979), as well as its corresponding coke formation model.

For feedstocks like E/P, which is an ethane and propane mixture, the reaction scheme was obtained by superposition of the schemes for single feedstock cracking which Froment and his co-authors had proposed in their papers (Sundaram et al., 1978). The cracking results, predicted by those kinetic data, give good agreements with the plant measurements. After such superposition, eleven component species and eleven free radical species are chosen to comprise a highly coupled eighty-two reaction network, which is listed in the Appendix A, for the cracking model. The following lists all the species involved in the cracking model.

Component:



Free radical:



Among them, C_5^+ is a lumped product of all the hydrocarbons heavier than C_5H_{10} .

3.1.2 Plug Flow Reactor Model

The one-dimensional Plug Flow Reactor (PFR) model is the model used here to study the component distribution and temperature distribution along the cracking tube in the radiant section. In a PFR, all reaction components are assumed to have a same residence or contact time. This residence time is calculated by the reactor volume divided by the volumetric feed rate at reactor average temperature and pressure. The concentrations of all the components and the temperature are assumed to vary only along the length of the tubular reactor; therefore, there is no radial distribution.

Two requirements need to be met in order to use this PFR model. One is that the ratio of length-to-tube diameter must be much greater than unity (i.e., $L/d_t > 20$). The other condition is that the flow must be turbulent (i.e., the Reynolds Number $Re > 2000$).

From the reactor configuration data, L/d_t , the length-to-tube diameter ratio, is approximately 100. Then, by using the Lucas's viscosity correlation equation listed in Appendix B, the Reynolds Number is in the order of 10^7 for the flow inside the tube. Thus, the one dimensional PFR model is suitable to be used to describe the temperature distribution and component distribution along the reactor. The model equations are:

$$\frac{dF_i}{dZ} = -\frac{\pi \cdot d_i^2}{4} \cdot \sum_j S_{ij} \cdot r_j \quad (3.3)$$

$$\frac{dT}{dZ} = \frac{1}{\sum F_i C_{p_i}} [Q(Z)\pi \cdot d_i + \frac{\pi \cdot d_i^2}{4} \sum_i r_i (-\Delta H)_i] \quad (3.4)$$

where

F_i = molar flow rate of the i-th component, mole/sec

d_i = tube diameter, m

S_{ij} = stoichiometric coefficient

r_i = reaction rate, $\text{mole}/m^3 \cdot \text{sec}$

Z = axial reactor coordinate, m

C_{p_i} = heat capacity of i-th species, $\text{kJ}/\text{mole} \cdot K$

$Q(Z)$ = heat flux, $\text{kW}/m^2 \cdot \text{sec}$

T = temperature, K

ΔH_i = heat of reaction, kJ/mole

Since not all the initial values for the differential equation networks are known, the measurement data from plants will be used to estimate some process parameters. This is called parameterization. The detailed approach for the model parameterization is discussed in Section 3.1.3, Pressure Distribution Calculation, and Section 3.1.5, Heat Transfer Correlation.

The effective heat transfer to the tube, $Q(Z)$, is parameterized by the coil outlet temperature measurement from the plant. After the heat supply load to the tube is fixed, the tube is divided into twenty sections. For each section, the kinetic data are assumed to be constant. Those kinetic constants are calculated from the average temperature of each section by an estimation of actual section inlet temperature plus one-half of the temperature increment of the section. That incremental temperature is taken from the previously determined section.

For such Ordinary Differential Equations (ODE's), high stiffness is detected since the time constants of the radicals are much faster than those of the molecular species. Also, the species are highly coupled in the reaction network. Livemore Solve for Ordinary Differential Equations (LSODE) integration package is very effective for solving such stiff first-order differential equations.

The advantage of LSODE comes from using a variable order and a variable integration step size (Riggs, 1994). The order of its implicit integrator will be decreased during the integration when several error tests are successful. At the same time, the step size will be adjusted to meet the convergence criterion. In this way, the software will find the best approach to integrate the ODE's because the optimized integrator order and step size are used.

3.1.3 Pressure Distribution Calculation

For this gas flow in the tube, a momentum balance is employed to describe the pressure distribution along the reactor (Bennett, 1974). That is,

$$\frac{dP}{dL} = -G \cdot \frac{du}{dL} - 2 \cdot \frac{f_r}{\rho \cdot D \cdot g_c} \cdot G^2 \quad (3.5)$$

where

D = tube diameter

u = average velocity of gas

f_r = pressure drop factor

G = mass velocity ($\rho \cdot u$).

For this differential equation, several simplifications are used to derive an explicit solution. First, the whole tube is divided into twenty sections while the mass velocity, G , is assumed to be constant for each section. Second, for each section, since the inlet and outlet temperature do not vary significantly, the isothermal state equation $\rho = \rho_0 \cdot \frac{P}{P_0}$ is applicable. By using the isothermal state equation, replacing u with G/ρ and assuming c_f maintain constant, the equation is rearranged to

$$\rho \cdot \frac{dP}{dL} - G^2 \cdot \frac{dP}{P \cdot dL} + 2 \cdot c_f \cdot \frac{G^2}{D \cdot g_c} = 0. \quad (3.6)$$

Integrating from a starting point, (e.g., the inlet of each section, $P = P_0$), while the distance of each section is ΔL , the pressure drop for a constant c_f is:

$$\frac{P_0^2 - P^2}{2} = G^2 \cdot \frac{P_0}{\rho_0} \cdot \left(\frac{2 \cdot c_f \cdot \Delta L}{g_c \cdot D} + \ln \frac{P_0}{P} \right). \quad (3.7)$$

When the pressure drop is less than 10% of the inlet pressure of each section, the term of $\ln \frac{P_0}{P}$ can be neglected:

$$P^2 = P_0^2 - 4 \cdot G^2 \cdot \frac{P_0}{\rho_0} \cdot \frac{c_f}{g_c} \cdot \frac{\Delta L}{D}. \quad (3.8)$$

After rearranging, the pressure equation is:

$$\frac{P}{P_0} = \left(1 - \frac{4 \cdot G^2}{\rho_0 \cdot P_0 \cdot A_c} \cdot \frac{c_f}{g_c} \cdot \frac{V}{D}\right)^{1/2} \quad (3.9)$$

where $\Delta L = \frac{V}{A_c}$.

For a real process, the outlet pressure has to be maintained at a certain value to make sure of the downstream's normal operation. To achieve this and to maintain the flow rate, the inlet pressure, which can be determined by solving the above equation, has to be increased as time progresses:

$$P_{in} = B + \sqrt{B^2 + P_{out}^2} \quad (3.10)$$

where

$$B = 2 \cdot \rho_{ave} \cdot u_{ave}^2 \cdot \frac{c_f}{g_f} \cdot \frac{\Delta L}{D}.$$

Here, ρ_{ave} = the average density flow inside each section

u_{ave} = the average velocity of flow inside each section

g_f = Newton-law proportionality factor for the gravity force unit.

Both plant measurement data and simulation results are consistent with the analysis.

The pressure drop factor consists of two parts: friction loss factor and duct loss factor. Friction loss factor is used to determine the pressure drop due to fluid viscosity. This frictional loss is a result of momentum exchange between the molecules in laminar flow or between the particles moving at different velocities in turbulent flow.

For fluid flow in conduits, frictional pressure loss can be calculated by Darcy equation:

$$\Delta P_f = 0.5 \cdot f_r \cdot (1000 \cdot L / D_h) \cdot \rho \cdot v^2 \quad (3.11)$$

where

ΔP_f = friction losses in terms of total pressure, P_a

f_r = friction factor

L = duct length, m

D_h = hydraulic diameter, mm

v = velocity, m/sec

ρ = density, kg/m^3 .

Within the region of the laminar flow (Reynolds number less than 2000), the friction factor is a function of Reynolds number only. For turbulent flow, the friction factor could depend on Reynolds number, duct surface roughness and internal protuberances. Colebrook's nature roughness function is used for the f_r calculation:

$$f_r = \left[\frac{1}{1.14 + 2 \cdot \log(D'/\varepsilon) - 2 \cdot \log(1 + \frac{9.3}{Re \cdot \varepsilon/D \cdot f_r^{0.5}})} \right]^2 \quad (3.12)$$

where

ε = tube roughness, mm

D = tube diameter, mm .

Once a flow reaches a fully rough area (i.e., the flow has a sufficiently large Reynolds Number and a certain level of roughness), the friction factor becomes independent of Reynolds number and only depends on the tube relative roughness and the third term in the denominator can be neglected. In modern ethylene plants, the assumptions of large Reynolds Number and fully rough flow are almost always true and the friction factor is calculated by a simplified equation:

$$f_r = \left[\frac{1}{1.14 + 2 \cdot \log(D/\varepsilon)} \right]^2. \quad (3.13)$$

The duct loss factor shows the pressure loss caused by fittings located at entries, exits, transitions, and junctions. This duct loss, caused by changing area and direction of the duct, is written as

$$\Delta P_f = 0.5 \cdot C' \cdot \rho \cdot v^2 \quad (3.14)$$

where

C' = local loss coefficient, dimensionless

ΔP_f = fitting total pressure loss, P_a

ρ = density, kg/m^3

v = velocity, m/s .

Those local loss coefficients can be checked by tables, curves and equations and each fitting loss coefficient must be referenced to that section's velocity pressure. For the elbow and an Y convergence tube, the local loss coefficient in *American Society of Heating, Refrigerating and Air-Conditioning Engineers' Handbook* are:

$$C_{elbow} = 1.3 \quad (3.15)$$

$$C_y = 0.32 . \quad (3.16)$$

Total pressure loss factor in one section of a tube is calculated by combining both friction factors and local loss factors. For a total section pressure drop:

$$\Delta P_f = 0.5 \cdot \left(\Sigma C + \frac{1000 \cdot f_r \cdot L}{D_h} \right) \cdot \rho \cdot v^2 \quad (3.17)$$

where ΣC is the summation of local loss coefficients within the tube section.

From the initial pressure drop measurement from the plant, linear pressure drop is assumed to begin the first iteration loop to calculate the component distribution and temperature distribution, which can then be used to improve the estimate of the pressure distribution. The new adjusted pressure distribution is used to re-calculate the reactor distribution and this process repeated until the variance of the nearest two pressure drop calculations falls into the convergence criterion.

By using this trial-and-error method, the initial pressure distribution is fixed and can be used to determine the value of the pressure drop factor for each section of the tube. Since the shut down pressure drop of the tube is no more than 10% greater than the initial pressure drop, the tube roughness can be assumed to be constant during the entire cracking run-length. By using this constant tube roughness and constant tube outlet pressure, the inlet pressure is calculated and found to have a slow but gradual increase during the entire run.

3.1.4 Coke Formation Model

Dehydrogenation of hydrocarbons occurs during the cracking. With a complete dehydrogenation, coke is slowly but continuously produced on the internal surfaces of the

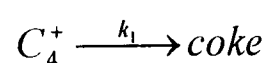
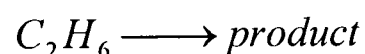
pyrolysis tube. The heavier the feedstock, the more the coke formed. Besides that, the waste particles, flowing with the liquid feedstocks even after some pretreating process, also tend to condense in the transferline exchanger and through some future reactions solidify on the internal surfaces of the tubes. These will reduce the heat transfer from the tubes to gases. In order to maintain the cracking rate, the flow rate of the fuel gas has to be increased and at the same time the tube skin temperature is slowly increased. This tube skin temperature will reach a maximum allowable value as the coke layer increases its thickness. The coke deposit may also result in a considerable increase in the pressure drop between the inlet and outlet of the tube since the actual usable cross section of the tube is decreased. This will change the pyrolysis final yield because of an increased total pressure and an increased hydrocarbon partial pressure. The plant has to shut down the furnace and decoke once the maximum allowable temperature is reached. Furthermore, the surface metal of the tubes is slowly removed by either coking or decoking, leading to pitting and erosion, and a shortened run life of a furnace. In an ethylene plant, one furnace is always down for decoking work or repair work while all other furnaces are in the normal operation.

The maximum allowable temperature is determined by the metallurgy. The furnace needs to be shutdown for decoking if this temperature is reached. Decoking is accomplished by removing the coil from service and using a steam-air mixture to burn the carbon out of the coil. The steam-air mixture is heated to 900-1000 °C and is slowly reacted with the carbon to produce hydrogen and carbon monoxide. The amount of air added is gradually increased as the amount of carbon decreases, until decoking is complete.

Coking can be minimized by carefully controlling the coil-metal temperature, steam/hydrocarbon ratio and proper coil outlet conditions. In all ethylene plants, one common prevention method is adding high pressure dilution steam into cracking coils to maintain the wall temperature as high as possible while at the same time to reduce the coke formation rate. Some other methods to prevent coking are proposed by developing cast coils and alloys, which have a better creep strength property to resist coke build-up. This will increase both the furnace run-time and coil life because the coils are allowed to operate at their best efficiency during the cracking.

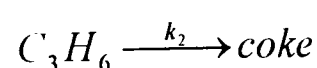
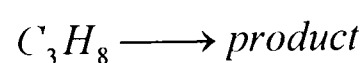
Much research has been done on the kinetic study of the coke formation model. Froment's research data is employed in the modeling work presented here.

For a pure ethane cracking, the following model scheme is proposed by Sundaram et al. (1981):



Then the coke formation rate is written as: $r_{cl} = k_1 \cdot C_{C_4^+}$ while $C_{C_4^+}$ is the sum of the concentration of all components heavier than C_3H_8 . The majority of C_4^+ in this work are butadiene and C_5^+ .

For pure propane cracking, the consecutive mechanisms are tested to be a most reasonable one (Sundaram et al., 1978). The reaction scheme is:



The coke formation rate is written as: $r_{c2} = k_2 \cdot C_{C_3H_6}$. The units for r_{c1} , r_{c2} are $(\frac{g \cdot coke}{m^2 \cdot sec})$.

Table 3.1 lists the kinetic data for coke formation model proposed in articles of Froment and his co-authors.

Table 3.1. Kinetic data for coke formation model

$E_1 (\frac{kcal}{mole})$	$A_1 (\frac{g \cdot coke}{kg \cdot i \cdot m^3 \cdot m^2 \cdot sec})$	$E_2 (\frac{Kcal}{mole})$	$A_2 (\frac{g \cdot coke}{mole \cdot i \cdot liter \cdot m^2 \cdot sec})$
28.25	8.55×10^5	73.58	5.82×10^{14}

Considering an E/P feed, each coking rate of pure feedstock is multiplied by its mole fraction in the feedstock mixture and summed to be the final coking rate for the process. In this manner, the data is fit to the coking result from the plant while no effort is needed to adjust the kinetic data. So the formation rate of the coke for the E/P feed is:

$$r = x_1 \cdot r_{c1} + x_2 \cdot r_{c2} \quad (3.18)$$

where

x_1 = ethane mole fraction in the feed

x_2 = propane mole fraction in the feed.

By using this coke formation model inside the tube, the increase in coke thickness Δt_c in time interval $\Delta Time$ in the reactor between z and Δz is:

$$\Delta t_c = \frac{(x_1 \cdot r_{c1} \cdot C_{C_4+} + x_2 \cdot r_{c2} \cdot C_{C_3H_6}) \cdot \Delta Time}{\rho_c \cdot 10^6} \quad (3.19)$$

where ρ_c is the coke density with a value of $1600 \frac{kg}{m^3}$.

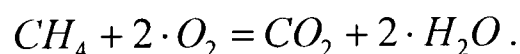
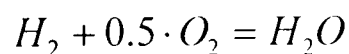
Since the coking yield is extremely small when compared to that of pyrolysis products, the coke formation rate can be considered as constant during a certain interval, $\Delta Time$. After each time interval $\Delta Time$, the tube diameter will be update by:

$$D_{t,new} = D_{t,old} - 2 \cdot \Delta t_c . \quad (3.20)$$

3.1.5 Heat Transfer Correlation

Thermal cracking process is a heat-driven process. The heat is supplied by the combustion of the fuel gas. The choice of the fuel depends on (1) availability, including dependability of supply, (2) convenience of use and storage, (3) cost, and (4) cleanliness. Since the top product of ethylene recovery tower is hydrogen and methane, which is generally used as nature gas, they meet all the four criteria to be the fuel gas in an ethylene plant. The combustion equipment is chosen by the state of the fuel gas. For this gaseous fuel, they could be burned in premix or diffusion burners which take advantage of the gaseous state.

The heat is supplied by the combustion of H_2 and CH_4 with air, which supplies sufficient oxygen. The combustion reactions are:



The way to calculate the reaction heat is supplied in the Appendix C.

The actual heat supply to the tube, used in the model, is adjusted to match the plant coil outlet temperature. This is another trial-and-error procedure, which is similar to

the pressure distribution adjustment calculation. In this way, the fire box simulation is omitted in my research work.

The tube skin temperature in the model is calculated by the principles of the heat flow. In the energy balance equation, the heat flow is dominated by conduction behavior while the radiation part is neglected here. For a steady state heat transfer by conduction in solids, Fourier's Law is:

$$\frac{dq}{dA} = -k \cdot \frac{\partial T}{\partial n} \quad (3.21)$$

where

A = area of isothermal surface

n = distance measured normally to surface

q = rate of heat flow across surface in direction normal to surface

T = Temperature

k = proportionality constant.

The proportionality constant, k , is a physical property of the substance called the thermal conductivity. For small range of temperature, k may be considered constant. For larger temperature range, the thermal conductivity can usually be approximated by:

$$k = a + b \cdot T \quad (3.22)$$

where a and b are empirical constants, T is the absolute temperature.

When this basic equation is applied into a cylinder, the heat transfer rate is:

$$q = -k \cdot \frac{dT}{dr} \cdot 2\pi r L \quad (3.23)$$

where

r = cylinder radius

L = cylinder length

k = thermal conductivity.

Assuming the temperature of the outside surface is T_0 , and that the inside surface is T_i and integrating the rearranged equation gives:

$$q = \frac{k(2\pi L)(T_i - T_0)}{\ln(r_0/r_i)} \quad (3.24)$$

where

T_0 = outside surface temperature for a cylinder

T_i = inside surface temperature for a cylinder

r_0 = outside radius of a cylinder

r_i = inside radius of a cylinder.

The cracking tube can be considered as a hollow cylinder composed of a series of layers, as shown in Figure 3.3. One layer is the tube metal with a constant thickness and another one is the coke layer which gradually increases in thickness. The empirical constants of the thermal conductivity for the tube material and the coke are given in Table 3.2. The temperature of tube skin can be calculated by solving the above equation.

Table 3.2. The empirical constants for the thermal conductivityd

	a	b
Tube ($W/m \cdot K$)	-1.2570	$4.327 \cdot 10^7$
Coke ($W/m \cdot K$)	6.4600	0.0

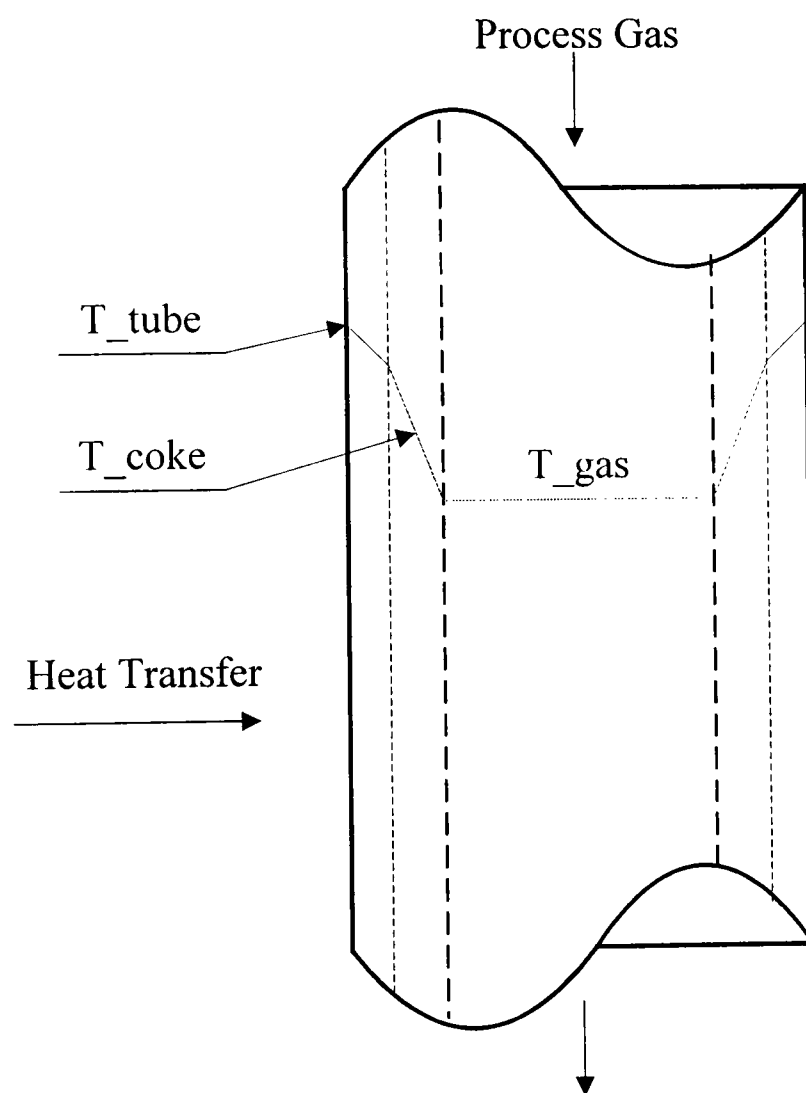


Figure 3.3. Tube heat transfer diagram.

3.1.6 Furnace Simulation and Benchmark Result

Figure 3.4 to Figure 3.12 show the model results after benchmarking against industrial data. Those results are considered to be proprietary information and only revealed here in dimensionless form.

The iteration time for the first two parameterization loops depend on the initial guess and the convergence criterion. Once the heat flux to the tube and the initial pressure distribution are generated, the whole furnace simulation CPU time will be less than 10 minutes with the assumptions of constant pyrolysis effluent flow rate and composition.

Figure 3.4 shows the component species distribution along the reactor. The desired product is ethylene, which amounts to approximately 30 mole% of the total pyrolysis gas. Hydrogen is another major product, based on its mole flow rate. Propylene and methane also occupy a considerable amount of the final product. The conversions for ethane and propane feeds are 54.6% and 92.9%, respectively.

Figure 3.5, which uses the same reference flow rate as the one in Figure 3.4, shows the free radical species distribution along the length of the reactor. The range of y axis in Figure 3.5 is from 0 to $4 \cdot 10^{-5}$, which indicates much lower concentrations of the free radicals inside the tube.

Figure 3.6 shows the pyrolysis gas temperature distribution along the reactor. From the figure, the furnace has a higher temperature increase at the beginning section of the tube than that at the end section of the tube.

Figure 3.7 shows the adjusted initial pressure distribution against the linear pressure drop assumption. Except in the elbow region and the wye converging fitting, the adjusted initial pressure profile is close to the linear one, so that parameterizations of the

heat flux and the tube relative roughness are iterated separately. Cascading those two loops will not get more accurate simulation results, but will slow down the convergence speed.

Figure 3.8 is the comparison of the predicted tube outlet effluent with the plant measurement data. This benchmark work demonstrates that the model is reasonably accurate considering that the rate constants are not adjusted to match the plant data. Although there is some model-prediction mismatch in the hydrogen product, the main product prediction is quite accurate while one considers that only published kinetic parameters are used. The hydrogen and methane are recycled to the furnace and used as the fuel gas, which is not included in the objective function. Other simulation results, e.g., the maximum coke thickness at the shut down time, the total run-length and the residence time, are also in a good agreement with the plant operation data, which are shown in Table 3.3 in dimensionless form.

Table 3.3. Furnace benchmark results.

	Max coke thickness	Run length	Residence time
Plant	≈ 1	≈ 1	0.83 – 1.0
Simulation	1.1	1.06	0.9

The ethylene profile for the reactor does not change significantly over the length of a run from the starting to shutdown as shown in Figure 3.9. Less than 1% changes are observed from the Figure 3.9, which are negligible for the process. Other components in

the reactor also have this negligible small concentration changes and are reasonable to assume that they are constant during the entire run. That is the basis for the constant pyrolysis effluent composition and flow rate assumptions to shorten the program CPU time. In the simulation, once the actual heat load and initial pressure profile have been fixed, the program will record one set of data of the species profile and temperature profile and use them as constants during the entire run-length. Only coke formation model, pressure distribution and tube skin temperature have to be recalculated until they hit the shut down criterion. In this way, it takes about 20 CPU minutes to obtain the furnace simulation result, which is running in Unix system on a 300 MHz PC. Otherwise, it would take more than 10 hours to get a similar result.

Figure 3.10 shows the coke thickness distribution along the reactor for the entire run. The coke is slowly but gradually deposited inside the tube, which causes the shut down of the furnace and decoking when the coke buildup becomes excessive. The maximum coke is located in the last section of the tube.

Figure 3.11 shows the pressure distribution along the reactor for the entire run. In order to maintain a normal operation in the downstream, the outlet tube pressure is kept constant while the inlet tube pressure has a slow increase with the coke thickness. The pressure drop at the shut-down time is about 17% greater than the initial value. The discontinuity of the pressure profile is caused by the tube design.

Figure 3.12 shows the tube skin temperature distribution along the reactor for the entire run. This temperature is usually used as a shut-down criterion because of the metallurgy constraint. The maximum tube skin temperature is located in the last section of the tube, which is consistent with the position of the maximum coke thickness.

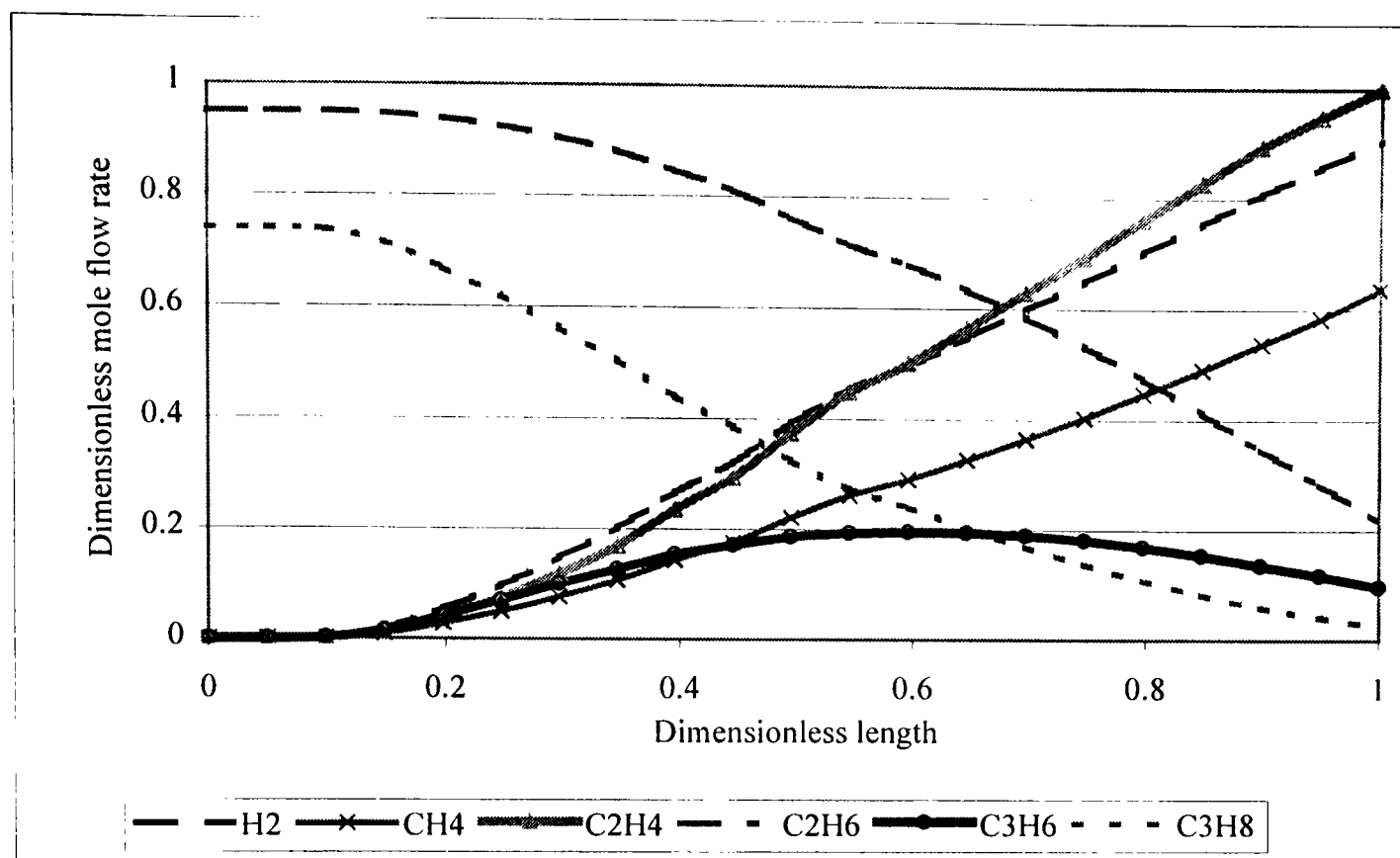


Figure 3.4. Component species distribution along the reactor.

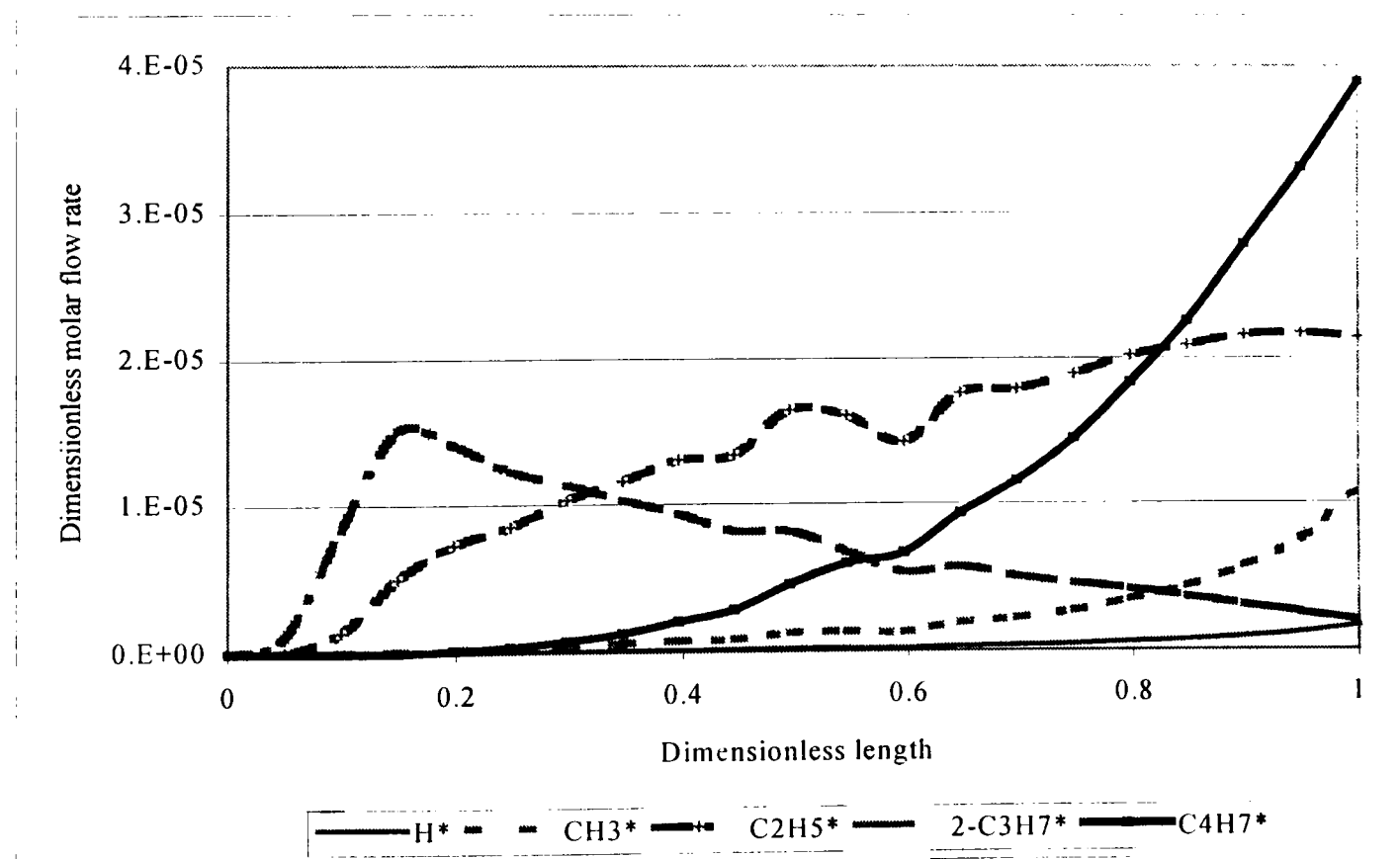


Figure 3.5. Free radical species distribution along the reactor.

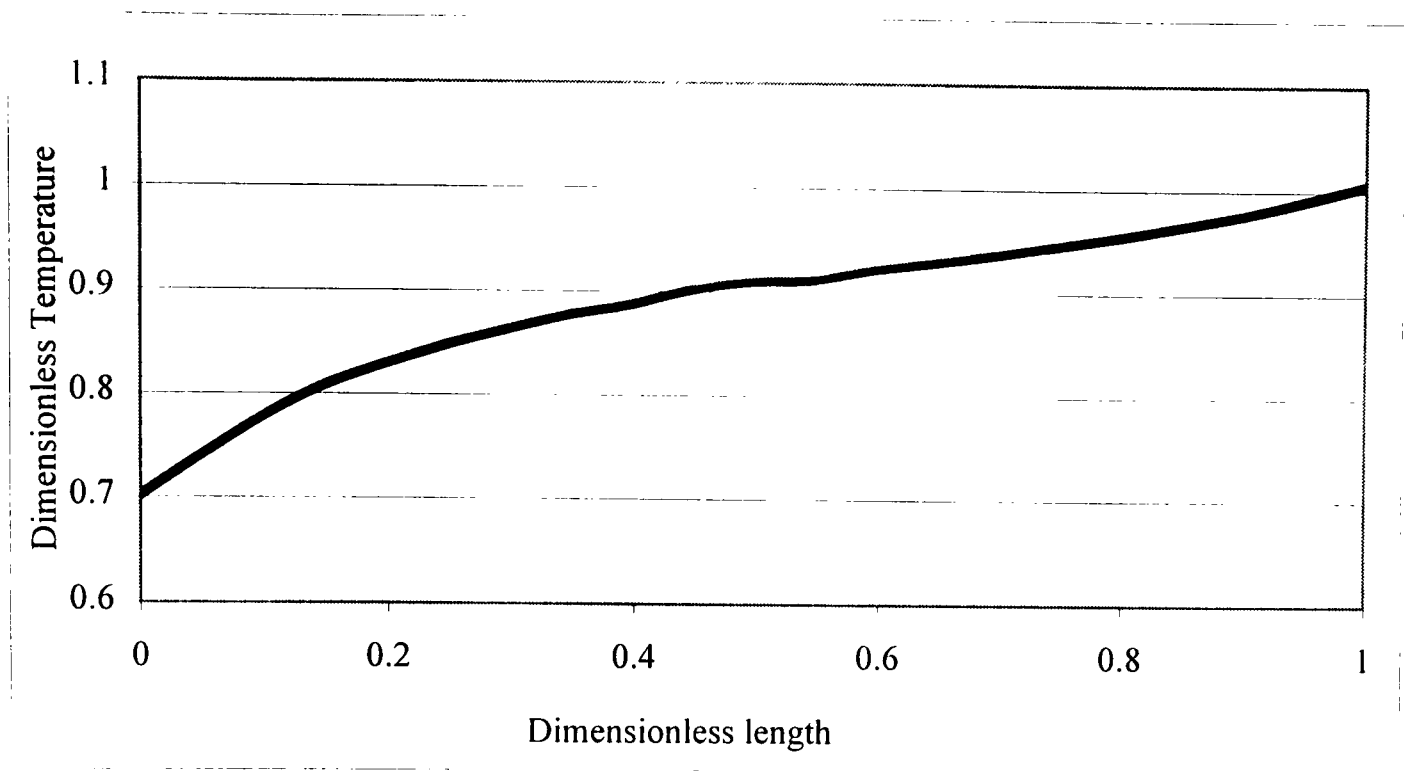


Figure 3.6. Temperature distribution along the reactor.

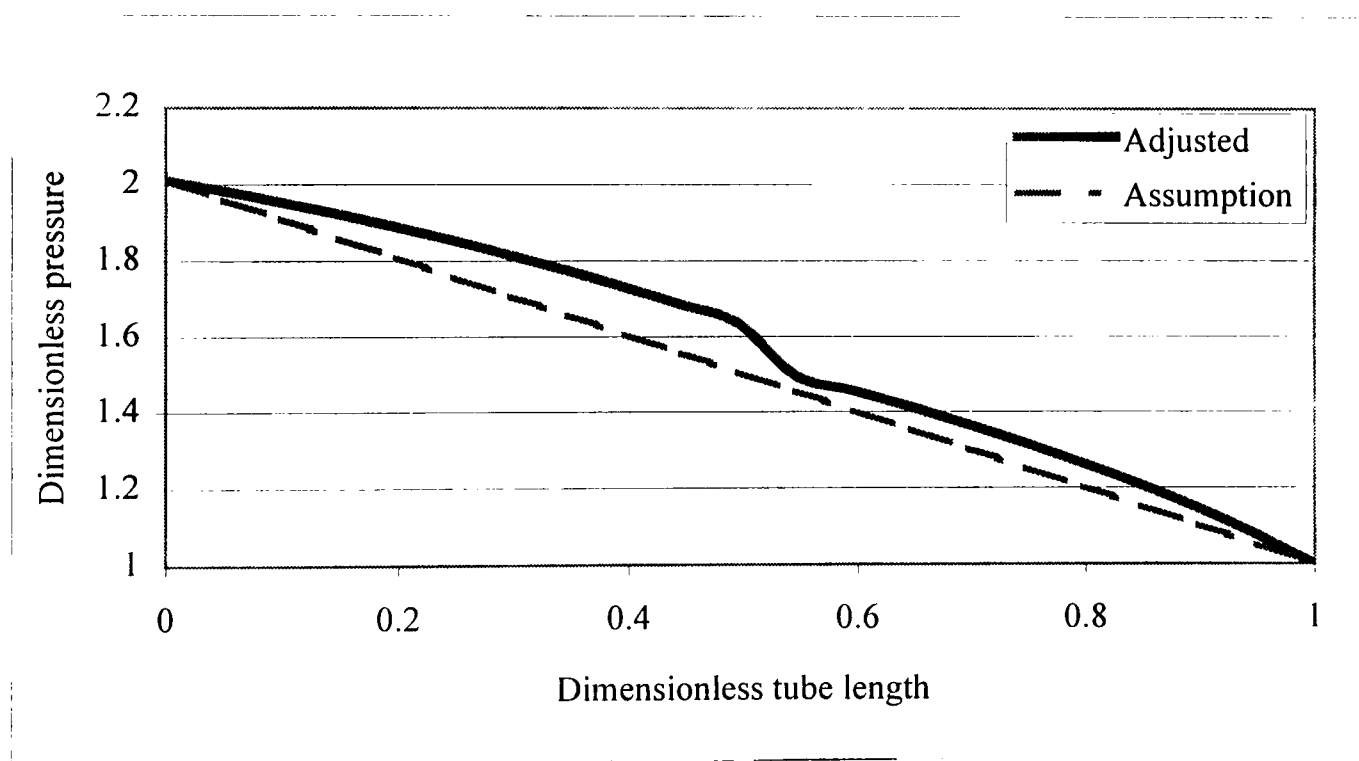


Figure 3.7. Initial pressure distribution versus linear pressure drop assumption.

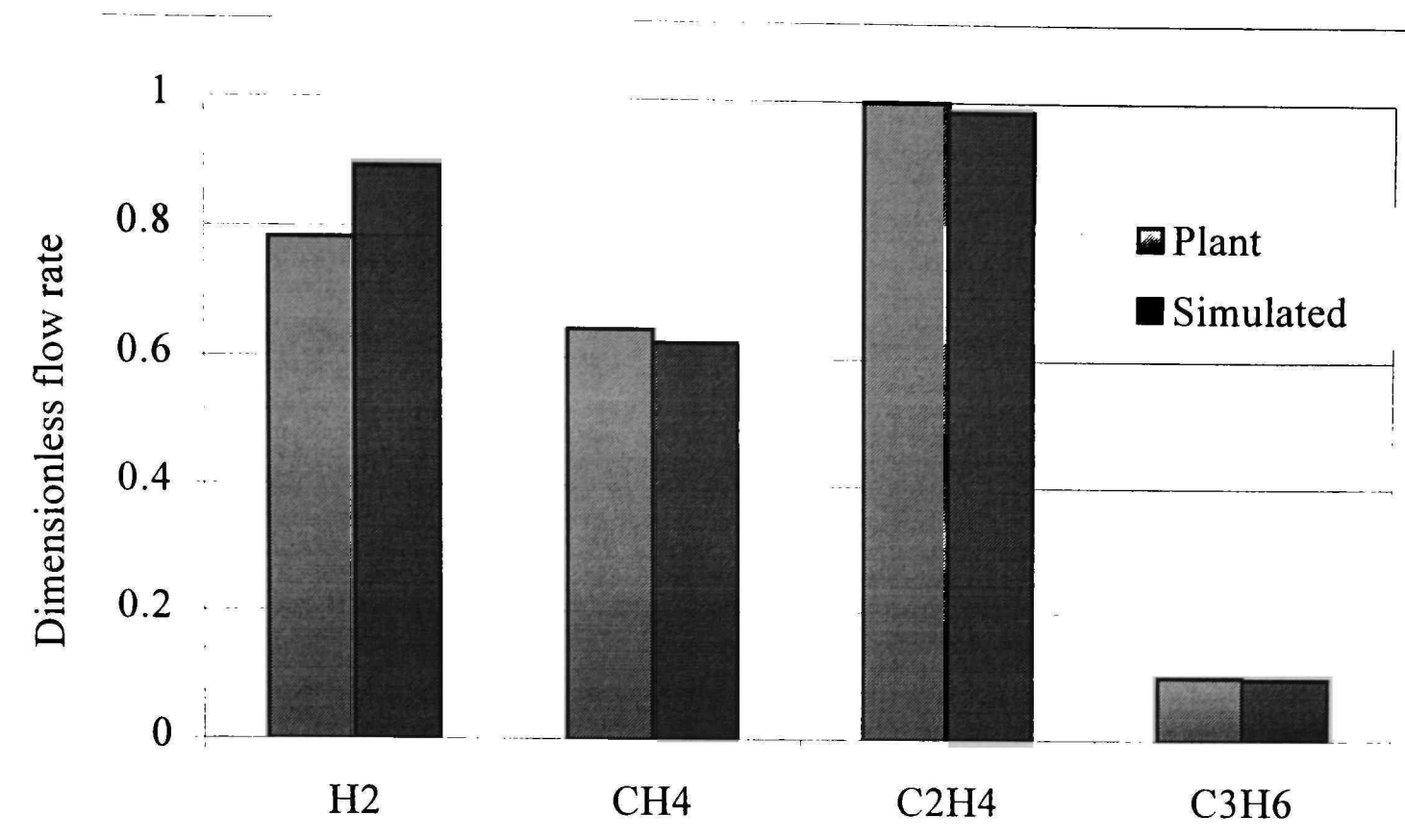


Figure 3.8. Benchmark result for the furnace effluent.

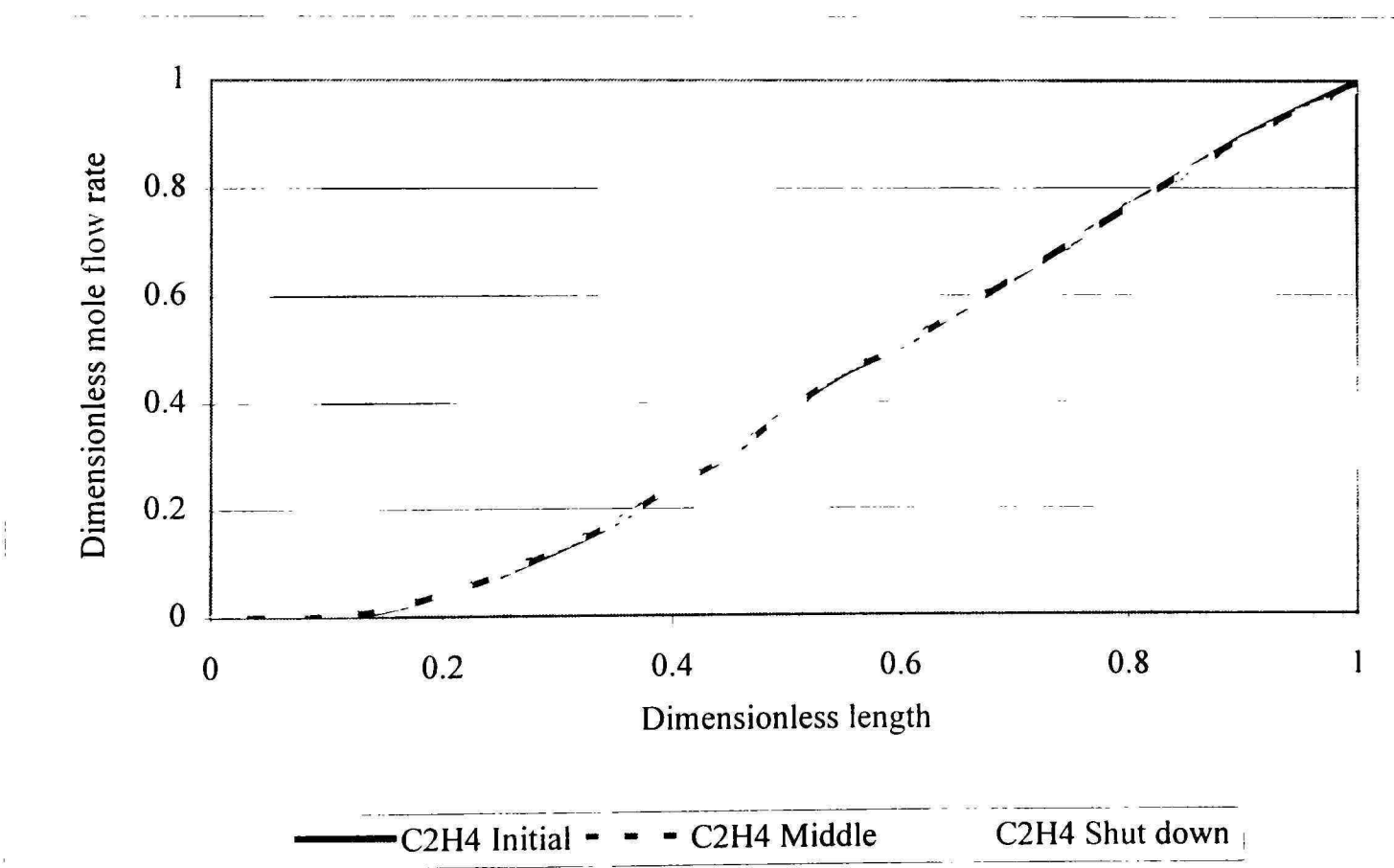


Figure 3.9. Ethylene product profile during the entire run.

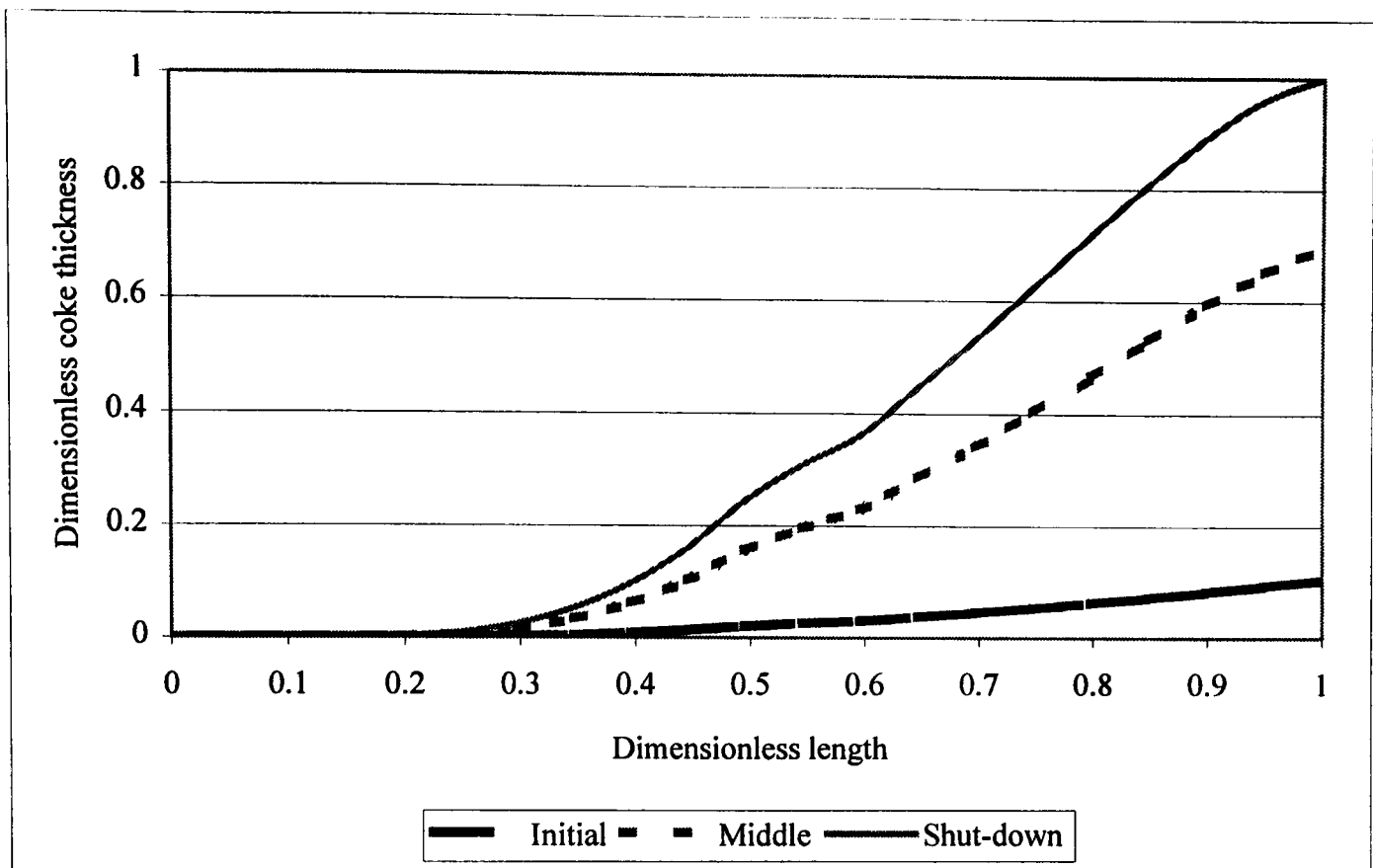


Figure 3.10. Coke thickness profile during the entire run.

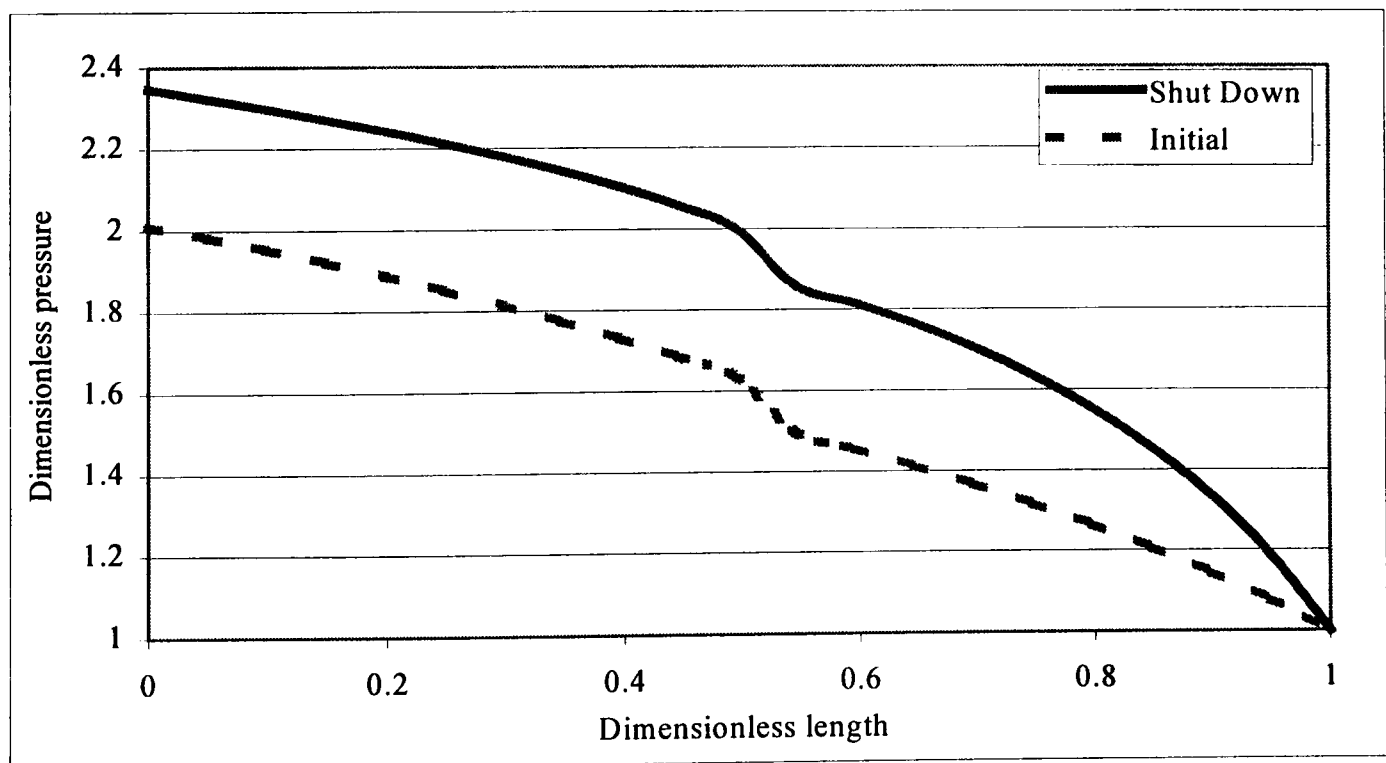


Figure 3.11. Pressure profile during the entire run.

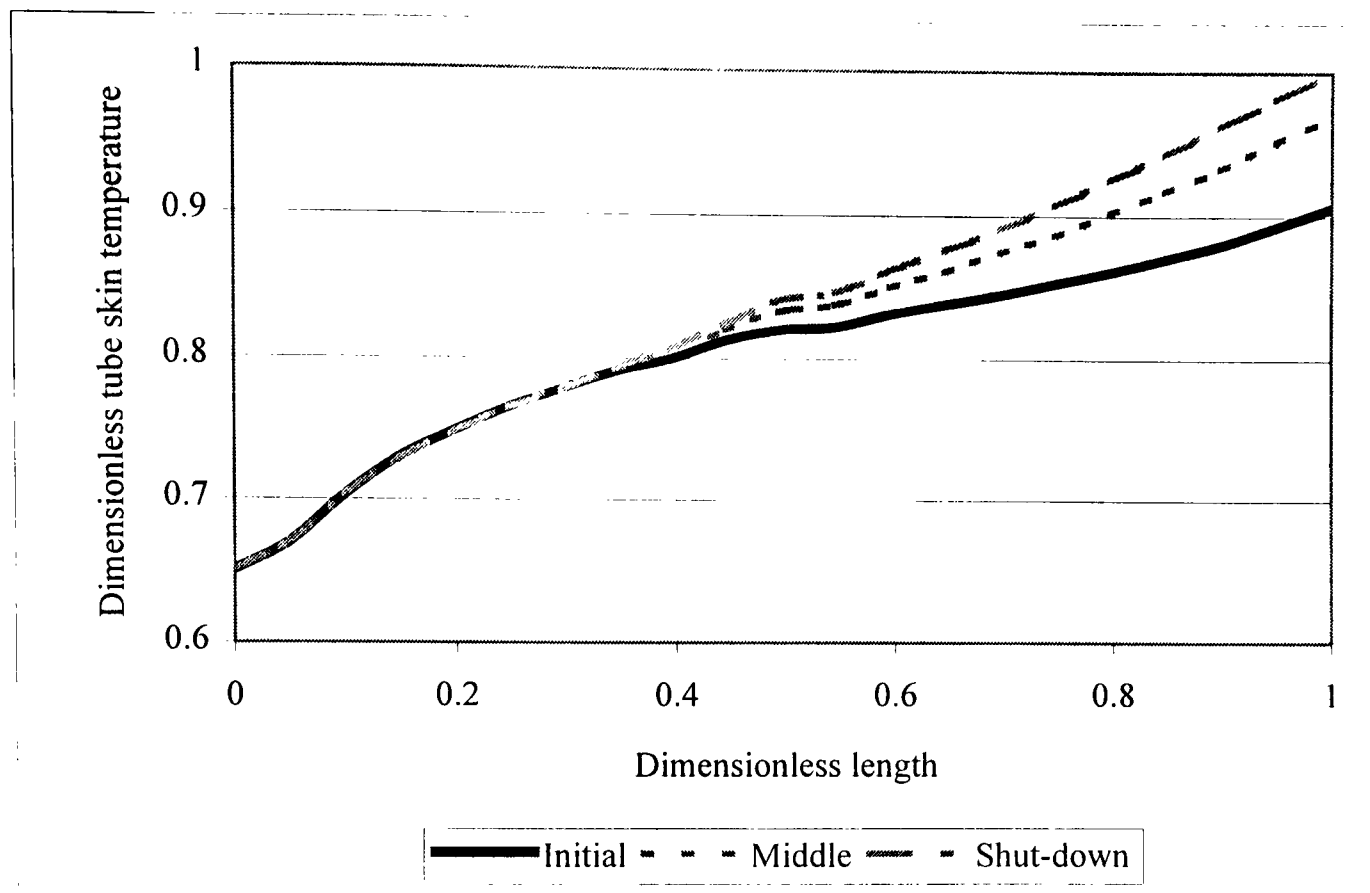


Figure 3.12. Tube skin temperature profile during the entire run.

3.2 Quench System

The pyrolysis gas from the cracking furnace is at a high temperature (e.g. generally 1200 °C for naphtha feed and 1150 °C for E/P feed) and further cracking reactions continually occur. To avoid producing more undesired by-product, the quenching system is used after the cracking furnace to abruptly decrease the cracking temperature.

Modeling of the waste heat reuse system was omitted in my modeling work because of the time limitation. Also, in my research, it was found that modeling quench system did not affect the final optimization result significantly. The following is just a brief introduction for this system.

3.2.1 Quench Process and Waste Heat Recovery

The quench system is such a device that consists of transfer-line exchangers (TLEs) to cool down the pyrolysis gas by using water or a suitable oil. The water used in this system is called quench water and the oil used is quench oil (Albright et al., 1983).

Quench water (Q.W.) is the condensed and physically treated steam and is contaminated with dissolved wastes. Usually, 150 psig steam is used in reboilers to boil off most of the Q.W. as the dilution steam to mix with the furnace feedstock. In addition to that, high-pressure steam can be generated by using quench water. This steam contains considerable heat that is reusable in down-stream processes or sold to other plants as a by-product.

The TLE used here can stop further pyrolysis reactions because it decreases the effluent temperature. Usually, this sudden temperature drop can be several hundred degrees, depending on the feedstock and operation conditions of the furnace.

Heat recovery is an important issue for efficient operation for an ethylene plant. Because the cracking process requires a certain fixed energy usage, it is more important to focus on the waste energy recovery for energy savings. In a modern ethylene plant, energy reusage can reach 91-93%.

Pyrolysis heat is mainly recovered in the convection section of the furnace and in the TLEs of the quench section. Cooling procedures employed by different plants vary widely. However, in order to obtain a higher waste heat recovery efficiency, direct oil quenching and direct water quenching are the best procedures. Direct oil quenching is based on direct injection of quench oil into the cracked gas. After the pyrolysis gas and quench oil are separated in a fractionation column, the gas at a temperature of 100-110 °C can be further cooled by direct water quenching. In direct water quenching, quench water absorbs the heat from the pyrolysis gas producing steam. The hot quench water needs to be separated from the heavy pyrolysis gasoline and is sent to various heat exchangers throughout the plant.

3.2.2 Tar Condensation

Coke formed in the cracking gas can flow with the stream and block the transfer-line exchangers' inlet tubesheet. This kind of blocking of the inlet tubesheet is called mushroom formation and is more prevalent on ethane feedstock. Besides, when the tube wall temperature is lower than the dew point of the pyrolysis tars, those tars will also

condense on the tube wall. These condensed high-boiling hydrocarbons are converted into a cokelike substance. Both coke and cokelike substances reduce the heat-transfer rate and increase the inner-surface temperature of the tube. So, TLE tubes must be cleaned periodically. High pressure water at about 500 to 700 atms is jetted into the TLEs' inlet tube to clean those tars. In industry, as a rule of thumb, it is always important to minimize tar condensation in the TLE (Albright, 1983), for example, the maximum cracking severity for Atmosphere Gas Oil (AGO) feed has to be limited to a minimum of 7 wt% hydrogen in the C_5^+ fraction (all the hydrocarbons heavier than C_5H_{10}).

Direct oil quenching and direct water quenching will remove the heavier tars and residuals from the pyrolysis gas and product gases are clean enough for the next compression stage.

3.3 Separation System

A separation system, largely composed of distillation columns, is used to separate the pyrolysis gases into the high purity final products.

3.3.1 Distillation Technology

Distillation is the most important and common separation technique in chemical engineering plants because it supplies the cheapest and best method to separate a liquid mixture to its components in most cases.

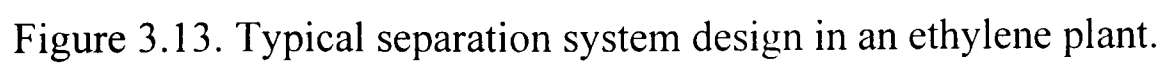
Distillation is the process of separating a mixture by using the differences in boiling points of the various components in the mixture. The lighter components, which have lower boiling point temperatures, mostly concentrate in the vapor phase at the top.

Similarly, the heavier components, which have higher boiling temperatures, are basically concentrated in the liquid phase at the bottom. Heat is added to the reboiler and removed by the condensor in order to affect the separation. Although distillation is not very efficient, thermodynamically, it is usually the most cost effective means to separate hydrocarbons mixture.

The pretreating is also very important to the distillation column's normal operation. Clay, salt, and other suspended solids must be removed from the feed before the distillation process to prevent corrosion and deposits. These materials are removed by water washing and electrostatic separation. Some plants use waste storage tanks to accumulate waste to separate the various waste streams prior to distillation.

3.3.2 Separation System General Design

For the separation system in an ethylene plant, a series of distillation columns are used to reach the required purity in the products. The organization of the distillation columns that comprise the separation system can vary widely from plant to plant. In this work, eight distillation columns are employed, including a demethanizer (DC_1), an ethylene recovery tower (C_2H_4 Recovery), a deethanizer (DC_2), a C_2 splitter, a primary depropanizer (HP DC_3), a secondary depropanizer (LP DC_3), a C_3 splitter and a debutanizer (DC_4). These distillation columns are all multistage columns and multicomponent systems except the C_2 splitter and the C_3 splitter, which are binary systems. Figure 3.13 represents the separation system design considered here. The feed, coming from the quench system, first goes to the primary depropanizer with a composition similar to the pyrolysis product.



3.3.3 Characteristics of Each Unit

3.3.3.1 Primary and Secondary Depropanizers. The effluent from the quench system goes to the primary depropanizer first. The high-pressure depropanizer works with the low-pressure depropanizer, a so called secondary depropanizer, to fractionate sharply into a C₃'s and lighter hydrocarbons fraction and a C₄'s and heavier hydrocarbons fraction.

The primary depropanizer works as a stripper with a moderate separation between C₃'s product and C₄'s product. The top product of the primary depropanizer goes to the demethanizer and the bottom goes to secondary depropanizer. C₃'s and lighter hydrocarbons have a high purity separation in the secondary depropanizer. This secondary depropanizer's top product goes back to the primary depropanizer and is used as part of the flux while the bottoms goes to the debutanizer. In this way, it can reduce the energy requirement of the depropanizer columns.

3.3.3.2 Acetylene Reactor. There are several ways to treat acetylene in the pyrolysis gas, depending on the concentration of acetylene and whether or not high purity acetylene needs to be recovered. For E/P feed, a moderate amount of acetylene is present in the top vapor flow of primary depropanizer. This top vapor flow passes over fixed catalyst beds and the acetylene will react with the hydrogen inside the vapor and convert to mainly ethane and partly ethylene.

This unit operation does not need be rigorously modeled since it is not a major concern in the whole plant. Generally, it accounts 0.4 mole% of the pyrolysis effluent

3.3.3.3 Demethanizer and Ethylene Recovery Tower. The demethanizer and the ethylene recovery towers work in a similar fashion to the HP DC₃ and LP DC₃ in order to

separate hydrogen and methane while reducing the energy consumption in the operation. The demethanizer works as a stripper for a moderate separation between hydrogen with methane and C_2 's with the heavier hydrocarbons. Its overhead product goes to the C_2H_4 recovery tower, while its bottoms product goes to deethanizer. At the top of the ethylene recovery tower, only a trace of ethylene is allowed in the off-gas, a hydrogen and methane mixture. This off-gas with a high combustion heat is recycled back to the furnace section and used as fuel gas. No further separation is needed for this off-gas mixture, which also reduces the separation cost of the plant.

3.3.3.4 Deethanizer. The deethanizer is a typical multi-component distillation column. It usually operates at a pressure of 2.4 to 2.8 MPa to separate the demethanizer bottoms products. Its overhead product is the feed to the C_2 splitter and its bottom is the feed to the C_3 splitter.

3.3.3.5 C_2 Splitter. A typical C_2 splitter contains 80 to 120 trays and requires a flux ratio of between 2.5 and 4.0, depending on the operating pressure and product specification. The ethylene-ethane mixture goes to the C_2 splitter for future separation to the desired final products, primarily ethylene in the top and primarily ethane in the bottom. Bottoms ethane will be recycled back to mix with the fresh feedstock and serve as feed to the cracking process. Top ethylene is sold in the market at different prices based on its purity.

3.3.3.6 C_3 Splitter. The bottom product of deethanizer is sent to a C_3 splitter. Due to the low relative volatility of propylene to propane, the separation of propylene from propane is even more difficult than the ethane-ethylene separation. To obtain a high-purity propylene, the column can have more than 300 trays, and is the tallest tower

among all these distillation columns. The overhead of C_3 splitter is another profitable final product: propylene, while the bottom product of propane can be recycled back to the furnace and be re-cracked

3.3.3.7 Debutanizer. The depropanizer bottom is further processed in the debutanizer for the separation of C_4 product from the light pyrogasoline. Debutanizer is a conversional fractionator with a steam heated reboiler and a water-cooled condenser. The operation pressure is a moderate one, approximately 0.4-0.5 MPa.

3.3.4 Approximate Model Approach

Before the 1950s, short-cut method was the commonly used calculation procedure since the calculation load is low. Even though the results were not as accurate as rigorous models, they are acceptable for this project. With the emergence of computer technology, rigorous models are primarily used to model modern plants.

The separation system, studied in this thesis, have adequate supplies of condenser duty and reboiler duty for each distillation column. Therefore, no constraints from the distillation columns result for the plant-wide optimization work and a rigorous tray-to-tray simulation is not needed here. The approximate model is suitable to simulate the final product and utility usage for this system.

The extended Jafarey equation is used to parameterize the average relative volatility throughout the column to match the base case data from the plant (Douglas et al., 1979). This average relative volatility is assumed to be constant during the simulation and optimization work and will be used to calculate new reflux ratios for the optimized operation.

The Jafarey equation for a binary system is:

$$N = \frac{\ln S}{\ln \left[\alpha \cdot \sqrt{1 - \frac{R + q}{(R + 1) \cdot (R \cdot z + q)}} \right]} \quad (3.25)$$

where

S = separation factor

R = reflux ratio

q = heat state of feed

α = relative volatility

z = light composition in the feed

N = column ideal stage number.

The separation factor for a binary system is

$$S = \frac{\left(\frac{x_{LK}}{x_{HK}} \right)_D}{\left(\frac{x_{HK}}{x_{LK}} \right)_B} \quad (3.26)$$

where

x_{LK} = light key mole composition in the product

x_{HK} = heavy key mole composition in the product

subscript B = bottom product of distillation column

subscript D = top product of distillation column.

This equation can be extended to a multicomponent distillation. Several lumping method have been proposed. The simplest one is to lump the light key and light nonkeys

into a pseudo-light-key component and the heavy and heavy nonkeys into a pseudo-heavy-key component, which is employed in this work.

The pseudo relative volatility, parameterized from the basecase data and pseudo-component of the feed, is also assumed to be constant during the whole optimization run and is used to recalculate the new reflux ratio for the next optimization work.

This equation is valid for a total condenser distillation column. But for a partial condenser, simply increase the number of the ideal stage by one and use the same equation.

Table 3.4, Table 3.5 and Table 3.6 give the general separation system design data, typical operation data and typical feed condition for the separation system respectively. In the table, N/A means no available. Table 3.7 shows some exemplary operation results.

Table 3.4. Separation system general design data.

Column	Total Stage	Feed Stage	Tray Efficiency
HP DC ₃	40	20	50%
LP DC ₃	70	53	60%
DC ₁	44	N/A	N/A
DC ₂	45	30	60%
C ₂ Splitter	100	20	70%
C ₃ Splitter	338	86	70%
DC ₄	40	20	60%
C ₂ H ₄ recovery	20	N/A	N/A

Table 3.5. Typical operation data for the separation system.

Column	Top T(F)	Top P(psia)	Bottom T(F)	Bottom P(psia)
HP DC ₃	-29	159.7	115	163.1
LP DC ₃	51	98	174	105
DC ₁	-88.4	191	-28.2	195
DC ₂	-51	145	74	149
C ₂ Splitter	-105	59.2	-56	159
C ₃ Splitter	101	231	123	253
DC ₄	103	62.5	241	66.1
C ₂ H ₄ recovery	-185.8	234	-128	236

Table 3.6. Typical feed condition for the separation system.

Column	feed T (F)	Feed P (psia)	Feed q value
HP DC ₃	10	162.7	0.03
LP DC ₃	115	163.1	0.866
DC ₁	N/A	N/A	1
DC ₂	-21	147	0.175
C ₂ Splitter	-79	65.2	0.3565
C ₃ Splitter	74	149	1
DC ₄	174	105	0.874
C ₂ H ₄ recovery	N/A	N/A	N/A

Table 3.7. Typical operation results for the separation system.

Column	Top LK recovery	Top HK recovery	Reflux Ratio
HP DC ₃	0.5202	0.3724	1.1308
LP DC ₃	0.9999	0.0139	1.6523
DC ₁	0.171	0.0646	N/A
DC ₂	0.9999	0.0114	0.5125
C ₂ Splitter	0.9985	0.0010	2.413
C ₃ Splitter	0.996	0.0024	23.46
DC ₄	0.893	0.004	1.822
C ₂ H ₄ recovery	0.886	0.0051	0.0766

3.3.5 Refrigeration System Model

In order to obtain the desired final products, several distillation columns are designed to fractionate the pyrolysis effluent. Some top products of the distillation columns require cryogenic temperatures to be condensed into a liquid state, in which external refrigeration systems have to be employed to reach such low temperatures.

The refrigeration system is a process to absorb heat from one place and reject it into another, through evaporation and condensation processes. The common example in our daily life is air-conditioning. The air-conditioner absorbs heat from the room and sends it to the outdoors. The simplest refrigeration cycle contains four processes and four thermodynamic states, which is shown in Figure 3.14.

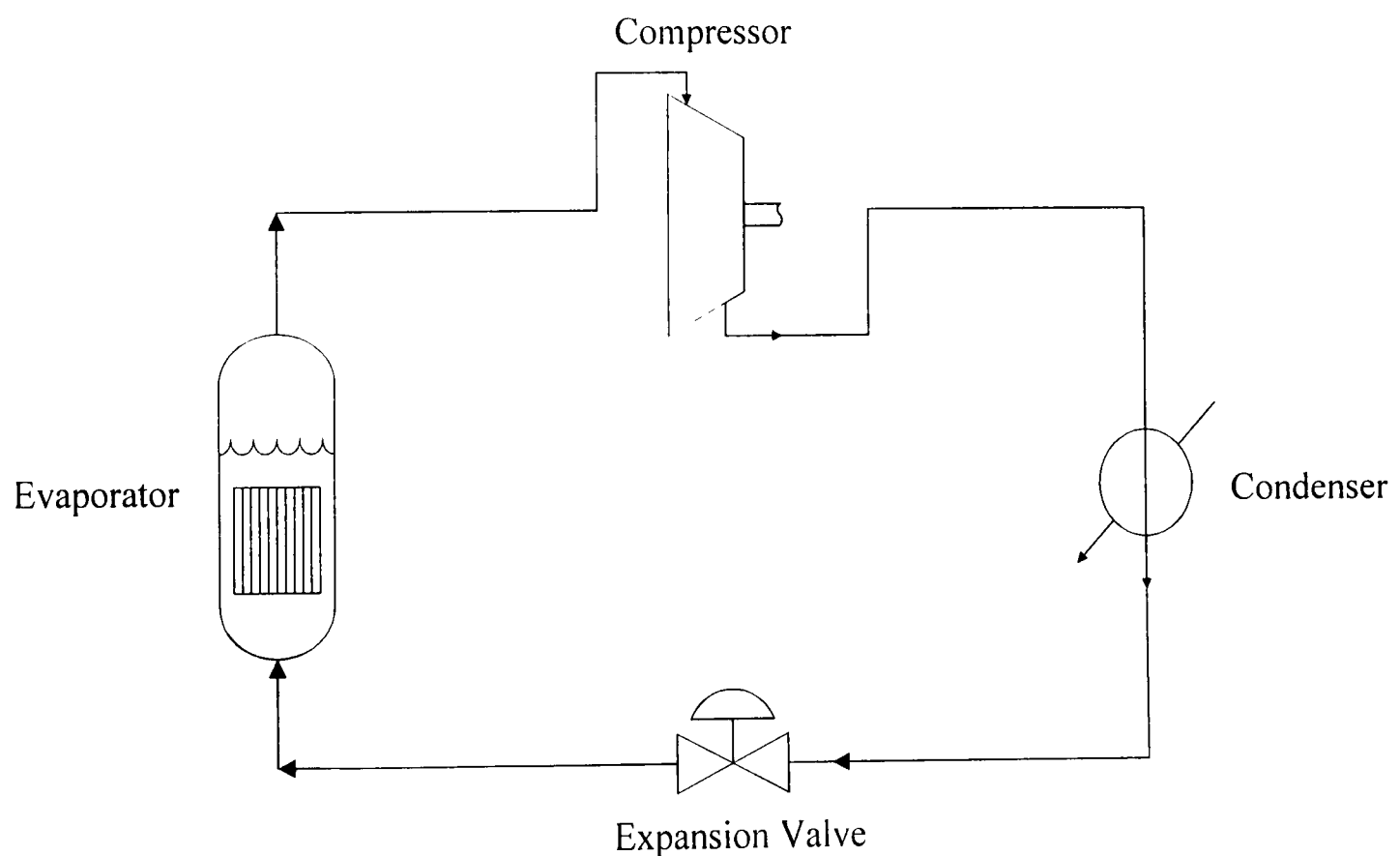


Figure 3.14. Simplest refrigerant cycle in a refrigeration system.

Process 1: Pure refrigerant vapor low pressure and low temperature (state 1) enters into a compressor, in which it is compressed into high pressure and high temperature vapor (state 2).

Process 2: That high pressure and high temperature vapor (state 2) goes into a condenser to be condensed into a vapor-liquid mixture at high pressure and low temperature liquid. With a special device or valve at the exit of the condenser. Only the liquid part of this mixture can go to the next process at a high pressure and low temperature (state 3).

Process 3: An expansion valve is used to continuously flash the refrigerant through decreasing the temperature of the liquid refrigerant.

Process 4: The low pressure and even lower temperature refrigerant (state 4) goes into an evaporator and evaporates there. Then, the part of pure vapor (state 1) could enter the suction valve of the compressor to repeat Process 1.

The refrigeration equipment design strongly depends on the properties of the refrigerant. To select a suitable refrigerant, one must consider many requirements, like the chemical stability under operation conditions, the non-flammability and low toxicity to fit specific applications. Cost, availability, and compatibility with compressor lubricants will also affect the final choice.

3.3.6 Refrigeration System in an Ethylene Plant

According to the availability criteria, ethylene and propylene are typically employed in the refrigeration system of the ethylene plant because they can cover the required temperature range. Other refrigerants, propane and ammonia, are occasionally

used to substitute for propylene. However, ethylene is an ideal choice as a refrigerant. Generally, the propylene refrigeration system has either three or four different levels while the ethylene system has two or three levels. Each level represents a different state of pressure and temperature. Table 3.8 and Table 3.9 give two ethylene refrigerant levels and four propylene refrigerant levels respectively. Adding to the number of stages in this cascaded refrigeration system will increase the construction costs and operation costs of piping line and heat exchangers, which is not economic for the plant.

Table 3.8. Two levels of ethylene refrigerant.

Stage	T (F)	P (psia)
First	-105.3	58.7
Second	-52.7	166

Table 3.9. Four levels of propylene refrigerant.

Stage	T (F)	P (psia)
First	-40	20
Second	2.9	50.7
Third	38.1	94
Fourth	68.5	148.7

The interactions between the refrigeration system and the separation system are modeled by a simplified approach and accurate results are obtained. The amount of refrigerant required is determined from the distillation columns' operating conditions, the feed rates and compositions, and the target products' qualities. Each level of refrigerant vapor flows to the corresponding refrigerant compressor, which represents the majority of the utility usage and sometimes even contributed to the plant's constraints. That is especially true for the cryogenic separation of hydrogen, methane, ethane and ethylene. Figure 3.15 shows a typical refrigeration system in an ethylene plant with four different stages.

Table 3.10 and Table 3.11 show the typical operation data for the ethylene compressor and propylene compressor, respectively, while the efficiency of each stage of the compressor is defined under normal operation conditions.

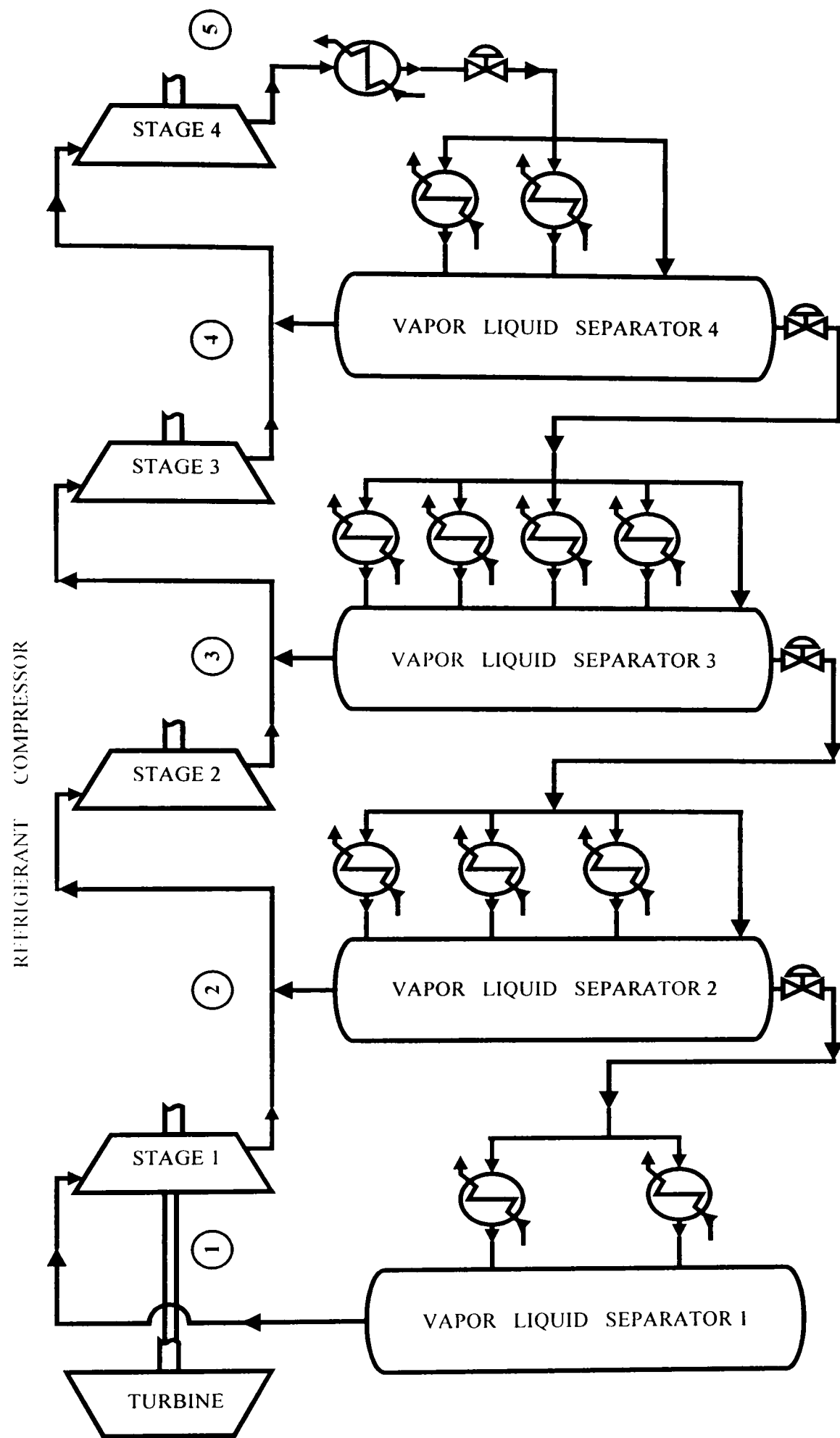


Figure 3.15. Typical refrigeration system design in an ethylene plant.

Table 3.10. Typical ethylene refrigerant compressor operation point.

	First stage	Second stage
Inlet T (F)	-105.3	12.2
Inlet P (psia)	58.2	165.4
Outlet T (F)	12.2	69.5
Outlet P (psia)	165.4	257
Efficiency	0.818	0.807

Table 3.11. Typical propylene refrigerant compressor operation point.

	First stage	Second stage	Third stage	Fourth stage
Inlet T (F)	-40.4	34	71	110
Inlet P (psia)	19.5	48.9	93.5	148.2
Outlet T (F)	36	87	115	163
Outlet P (psia)	50.2	93.5	148.2	247
Efficiency	0.852	0.846	0.810	0.770

3.3.7 Benchmark Result for the Separation System

Propylene and ethylene refrigeration systems in this work are effectively integrated with the separation system to calculate all the heat duty requirements, the flow rates of the refrigerants, as well as compressor horsepower usage. All the operation requirements are based on the normal operation of producing 50% of the ethylene vapor product at low pressure and 50% of the ethylene vapor product at high pressure. The heat duty calculation is based on the SRK equation, which is listed in Appendix D.

Compressor horsepower is supplied by a turbine which runs under high pressure steam.

Figure 3.14 shows seven comparisons between the simulated heat duty requirements and the plant data. Two sets of results agree with each other very well. Figure 3.15 shows the benchmark results for the refrigerants' compressor brake horsepower. The simulated results predict the plant data quite well. There exists some model-prediction mismatch, which is mainly caused by the simplified model used. Since some small units are ignored in the model, the simulated duty requirement for one level of refrigerant is less than the actual one. On the other hand, the physical properties of C_5H_{12} is used to calculate the heat duty requirement for the lumped product C_5^+ , which also causes a lower simulation value. However, on an overall basis, the separation system simulation agrees well with the plant data.

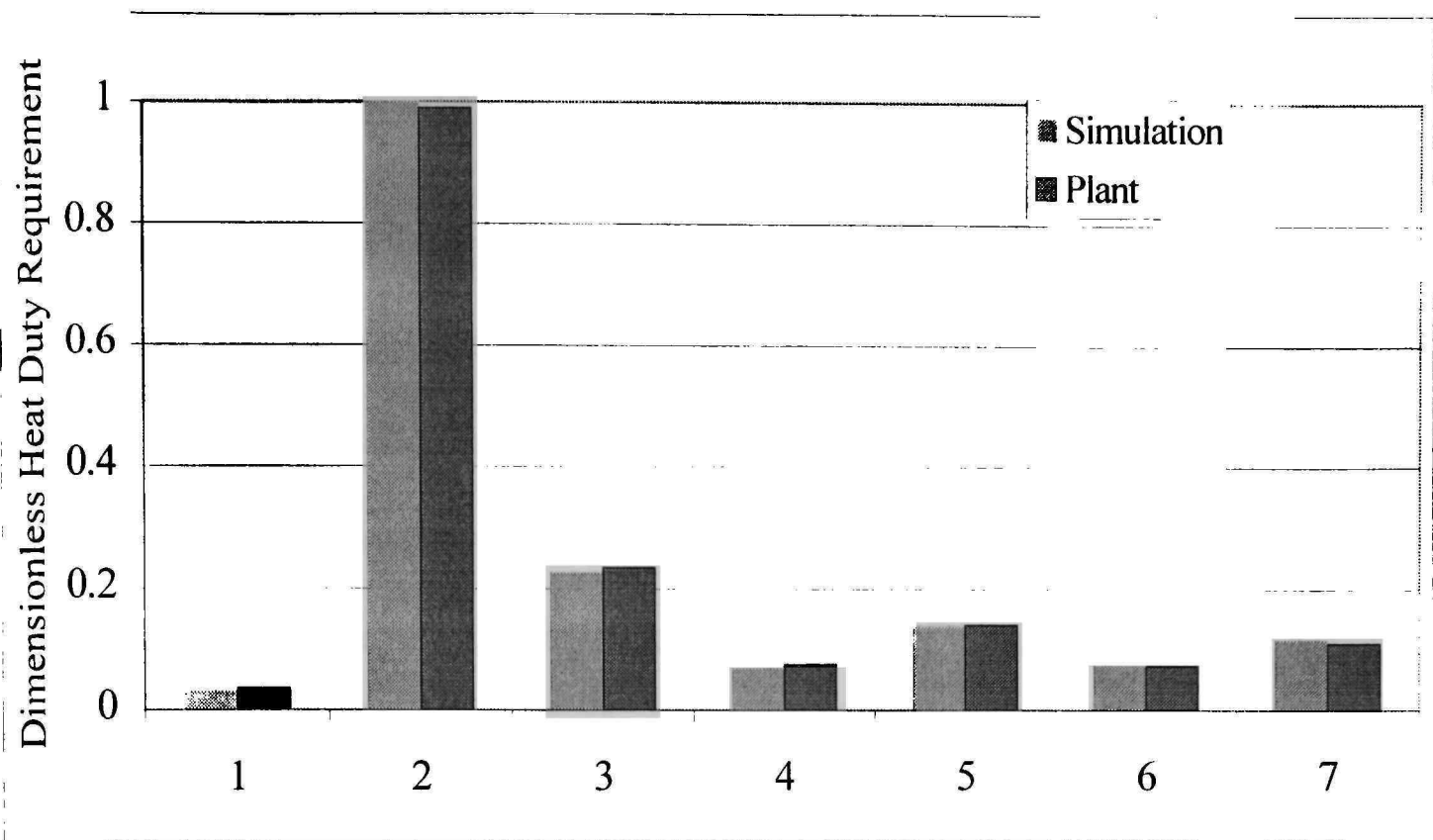


Figure 3.16. Heat duty requirement benchmark.

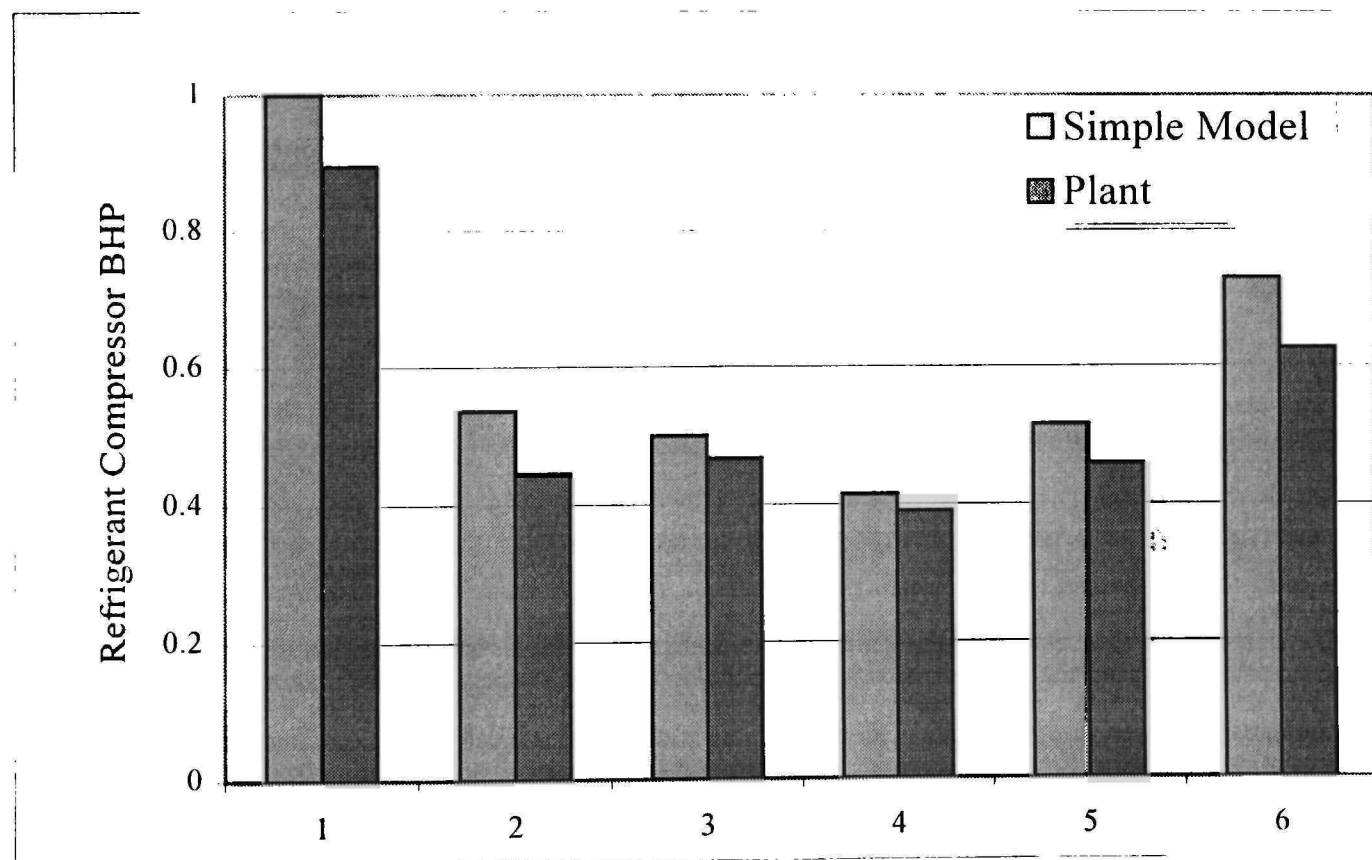


Figure 3.17. Refrigerant compressor BHP benchmark.

CHAPTER 4

OPTIMIZATION TECHNOLOGY

4.1 Chemical Industry Optimization

The finance in a manufacturing plant could be divided into several categories, raw material cost, energy cost, currency depreciation, tax, interest, and so on. For optimization of the existing chemical processes, only three types of variables require consideration: product value, feedstock cost, and utility usage. Usually, the objective function of a process is defined by the plant gross profit, which is:

$$\text{Profit} = \sum \text{Product Value} - \sum \text{Feedstock Cost} - \sum \text{Utility Cost},$$

which indicates that the major benefit comes from increased plant capacity, reduced energy requirements, and improved product quality.

Decision variables are those variables that are used to construct the entire process model and can be changed independently according to the operation. The independent variables are driven by the economic objective function to the optimal values. Decision variables are the setpoints left after control function has been satisfied.

The constraints are those bounds that should be honored by the process. The constraints can be divided into the following categories: linear and non-linear, equality and inequality. A huge manufacturing plant is always operated under multiple constraints. Some of them must be honored because of the safety consideration, such as the metallurgical requirement for the tube skin temperature. Some of them, like the distillation column product impurity limits, could have deviations but should be adjusted back to the setpoints by the control system. Choosing the correct constraint ranges is a

very important step for the optimization work because it can eliminate infeasible operation points and affects the safety of the operation in a plant.

In a modern chemical industry, Real Time Optimization (RTO) is very popular since it will provide the way to take care of all the plant operational changes and continuously drive the plant toward its optimum operating point. Since RTO runs automatically, no intervention or approval is required for set point changes from unit operators. Also, this system will complete all data transfer, optimization calculations and set points implementation before unit conditions still maintain in the steady state. The optimization system translates the economics of the chemical business into optimum operating setpoints which are implemented via the process control system.

In RTO technology, the process monitors collect the key measurements in the plant to check the steady-state status for the entire process. Once the measurements fall into the allowable deviation range, the entire process is assumed to be in steady state and all the required variables are used for the parameterization work for the modeling case. The changes in those parameters account for different operation cases, e.g., high severity vs. low severity reaction. After matching the current plant operation data by the parameter fitting, the optimization study starts to search the setpoints decision variables for the control system. The steady state condition of the plant needs to be rechecked before those optimized operation data are transferred to the control system. If the plant is still steady, then the controllers will drive the process to the desired values and reach another steady state. After a line-out period, the process detectors start a new cycle for the RTO strategy. This continuous and automatic updating of the process model in this RTO system is the characteristic difference from the off-line optimization approach.

The general approach for plant-wide optimization is to integrate all the major units into one flow sheet and implement all the decision variables and constraints simultaneously. Unit-optimization is choosing one process to search the optimal operation point. For example, selecting the optimal feed stage for the distillation column, or choosing optimal reflux ratio for the distillation column operation is the sub-unit optimization study. Some units may be operated under sub-optimal condition in order to obtain plant-wide optimization. Furthermore, sub-section optimization may give an unreasonable operation point to the downstream equipment or even violate the constraints of the downstream facilities; that can be the contrary to the overall plant objective.

4.2 Mathematical Formulate

The conceptual optimization objective function is posed as:

Minimize $P(X)$

subject to $f_i(X) = 0$

and $a \leq g_j(X) \leq b$

while $X_{lower} \leq X \leq X_{upper}$

where

$P(X)$: objective function

$f_i(X)$: equality constraints

$g_j(X)$: inequality constraints

a : lower bound for the equality constraints

b : upper bound for the inequality constraints

X_{lower} : lower bound for the model variables

X_{upper} : upper bound for the model variables.

4.3 NPSOL package

NPSOL (Gill et al., 1986) is an optimization software package which is developed by Stanford Business Software, Inc. It can effectively solve nonlinear constrained optimization problems with a global convergence to a minimum objective value by employing the most advanced searching method, Sequential Quadratic Programming (SQP). The mathematic estimations for the derivatives of the decision variables are generated if the user does not supply the numerical ones. NPSOL is more user-friendly because users just need to choose the decision variables and construct their own objective functions along with all the constraints. After supplying a set of initial guesses for the decision variables, this optimization package will automatically find optimal feasible solutions for the user-defined objective function.

The SQP used in NPSOL is the most advanced searching technology in the optimization study. It will successively convert the nonlinear problems into a quadratic programming problem which is solved at each iteration step; this makes sure the optimal values for the objective function will be mathematically found at the end of the search.

Scaling is very crucial for NPSOL to find correct answers. After scaling the decision variables and the objective function value, the step size to numerically estimate the first derivatives of the decision variables has a similar order to the searching step size.

During the running of NPSOL, several lines of output are produced after every major iteration. Those lines indicate the status of the optimization package at current

point. For example, a three-letter indication is generated to represent the status of the three convergence tests. After understanding the meaning of each letter, it is much easier to adjust the data in NPSOL Option file and head the search path to the right direction for the convergence.

CHAPTER 5

OPTIMIZATION STUDY

5.1 Characteristics of the Optimization Study

Based on the characteristics of the whole processes, the optimization in this work is defined as a plant-wide time-domain optimization. The major processes of the ethylene plant are modeled and benchmarked against the industrial data collected from a North American ethylene plant. The interactions between the separation system and the refrigeration system are accurately represented by a simplified model, which is derived from short-cut methods. Additionally, the utility cost, the electricity usage in the refrigeration system, are included in the objective function because refrigerant compressors represent the majority of the utility cost, and are often the main plant capacity constraint. The penalty of the furnace shut-down period for the decoking is also taken into account in the objective function. This time-domain objective function is

defined by $\frac{\text{Profit}}{\text{Day}}$:

$$\begin{aligned} \frac{\text{Profit}}{\text{Day}} = & \left(\sum \text{Product flow rate} \cdot \text{Product price} \right. \\ & - \sum \text{Feed flow rate} \cdot \text{Feed price} \\ & \left. - \sum \frac{\text{Utility usage}}{\text{Day}} \right) \cdot \frac{\text{Run-length}}{\text{Run-length} + \text{Shut-down}} \end{aligned}$$

Since the objective function is minimized, the $\frac{\text{Profit}}{\text{Day}}$ times negative one is evaluated by

NPSOL to search for the optimized operation point since NPSOL searches for a minimum.

As a highly integrated plant, the equipment is usually operated at multiple constraints when optimized. Typical constraints for an ethylene plant are coil outlet temperature, furnace heat supply limit, column flooding constraints, product impurity specifications, maximum or minimum production flow rate constraints and feedstock flow rate constraints. Some bounds must be honored completely, such as the maximum production flow rate permitted by the government authorities. Other absolute bounds could be the tube skin temperature, which is determined by the metallurgy limits, and the feedstock flow rate, which can be limited by the refrigeration system's total condenser duty supply. The process may deviate from the constraints, but will be driven back to their setpoints by a good control system. With the over-designed separation system, only the top or bottom separation factors are considered as the constraints, while the column flooding, the reboiler duty supply and other common separation system constraints are not considered in this work. The temperature and pressure operating data for the distillation columns in the separation system are taken from the base case, since they should not change greatly for the range of operation produced by the optimization algorithm.

Severity can be used as a constraint in the process, even though, theoretically, it is a result of the optimization process. For ethane and propane cracking, the severity is directly evaluated by the conversions of the feedstocks which are defined by the fractional disappearance of the reactants. Since the tube skin temperature cannot be accurately measured, the severity is used to indirectly indicate the coking rate inside the tube. High severity causes a higher frequency for decoking which increases the rate of aging of the furnace tubes and shortens their lifespan.

Since the design and geometry of an existing olefins plant are fixed, the major independent variables in the plant model could be the following parameters: conversion or severity of each furnace, steam-to-hydrocarbon ratio for each furnace, distillation column overhead separation, distillation column bottom separation, feedstock flow rate, feed composition, cracked gas compressor suction pressure and other model variables. Because of the prepriority nature of this part of data, the constraints and decision variables used in this work are not listed here.

One product may have several different values according to its quantity, quality and its final usages. However, since the contract price, market price and the inner plant price bear no significant differences, the price data used in the optimization study are selected from the publicized price sources, *Chemical Market Reporter*, from January, 1999 to September, 1999, which are listed in Table 5.1. The data listed in Table 5.2 are also from January, 1999 to September, 1999, which are supplied by another North American Olefins Company since they could be found in *Chemical Market Reporter*. From Table 5.2, we can see certain products' selling prices can undergo dramatic changes within six months which reflects the fluctuation of the oil business. In this work, the average price data from January, 1999 to September, 1999 are used to calculate the products credit and the feedstocks cost. The electricity cost rate maintains at a constant \$0.04/kW/hr.

Fuel gas price is usually determined by its heat supply when it is combusted into carbon dioxide and water at 25°C . Since the fuel gas in an ethylene plant is the recycled ethylene recovery tower top product, methane and hydrogen, it is reasonable to assume that all the fuel gas produced from the separation system is completely consumed by the

cracking section for the heat supply. Therefore, the fuel gas cost and the product credit of methane and hydrogen are omitted in the objective function.

For the lumped product of C_5^+ , the price depends on its final usage. It can be recycled back to pyrolysis gas and used as heavier feedstocks; it can be mixed with gasoline; or it can be used in other downstream equipment. The price for C_5^+ is assumed to be two or three cents less than that of the light hydrocarbon gasoline.

The two values, shown by ethylene and 1-butene in Table 5.1, represent the price ranges by the different suppliers, as well as differences in quantity, quality and location. The two values shown for propylene are the difference selling prices between polymer grade product and chemical grade product.

Table 5.3 lists the specific gravity for each product of Table 5.2, which is used to convert its price from cent/gallon to \$/lb. Suppose the specific gravity of H_2O (liquid) is constant: $1 \frac{gram}{cm^3}$, then after converting, Table 5.3 uses the same price unit as the one in Table 5.1.

Table 5.1. Price data I (unit: \$/lb).

Time	Ethylene	Propylene	Butadiene	1-Butene
Jan. 4	0.19/0.20	0.1275/0.1125	0.15	0.26/0.30
Feb. 1	0.19/0.20	0.1275/0.1125	0.15	0.26/0.30
Mar. 1	0.19/0.20	0.12/0.105	0.15	0.26/0.30
Apr. 5	0.19/0.20	0.12/0.105	0.13	0.26/0.30
May. 3	0.22	0.12/0.105	0.13	0.26/0.30
Jun. 7	0.21/0.2175	0.12/0.105	0.13	0.26/0.30
Jul.5	0.22/0.23	0.135/0.12	0.13	0.26/0.30
Aug.27	0.22/0.23	0.135/0.12	0.13	0.26/0.30
Sep.6	0.23	0.145/0.12	0.13	0.26/0.30
Ave	0.21	0.128/0.112	0.137	0.28

Table 5.2. Price data II (unit: cent/gallon).

Time	Ethane	Propane	n-C ₄ H ₁₀	Gasoline
Jan.	16.47	21.75	26.43	28.84
Feb.	18.32	22.43	27.01	28.11
Mar.	20.78	24.10	26.51	30.86
Apr.	27.95	28.26	31.42	35.21
May	28.05	28.31	32.15	35.92
Jun.	26.45	30.95	33.95	38.20
Jul.	28.45	37.26	42.17	45.27
Aug.	36.47	40.51	45.39	50.40
Sep.	34.89	42.88	47.82	53.06
Ave	26.426	30.716	34.761	34.43

Table 5.3. Specific gravity and converted price.

	Ethane	Propane	n-C ₄ H ₁₀	Gasoline
Specific gravity	0.585	0.564	0.621	0.60
Price(\$/lb)	0.05413	0.06741	0.06707	0.06875

Different processes could have different cycle times for implementing the optimization analysis because they have different dynamic response times. The response time for the furnace section can be 80 times faster than that of a C₂ splitter. Practically, the plant will use the hourly average of the previous measurements to check the steady state status and to prepare a parameter fitting case for the process model. After rechecking the steady state status, the optimization results can be implemented 4-6 times per day. The times of the optimization study implementation could be ideally applied more frequently, but the maximum cycle that can be used within one day is constrained by the most sluggish sub-unit in the plant.

5.2 Results of the Optimization Analysis

For the simplified model, qualitative optimization results are more reasonable than quantities results. Table 5.4 lists values of the decision variables used in the optimization study. Those decision variables are chosen according to their economic effects. Because of the propriety nature of these data, only the normalized data are shown here. From this table, same decision variable results are obtained for both the plant-wide optimization and the furnace sub-section optimization. Furthermore, the feedstock in the optimization result is driven to its upper limit and the optimal dilution steam to hydrocarbon ratio is found.

Table 5.4. List of decision variables.

Decision Variable	Base Case	Starting Point	Plant-Wide Optimization	Furnace Part Optimization
Feed flow rate	0.9365	0.9	1.0	1.0
DS/HC ratio	0.8	0.8	0.95	0.95

Figure 5.1 compares the economic differences between the base case and the optimal result. The numbers of 1, 2, and 3 in the x-axis represent the product credit, the utility cost, and the gross profit respectively. From the graph, the gross profit is increased about 6% after the optimization. The increase is coming from the increased feed flow rate. The separation utility usage is increased too because of the increased pyrolysis gas flow rate. However, the product credit can compensate the extra utility cost and obtain extra profit. Moreover, the run-length for the optimization result is doubled by the

increased the dilution steam to feedstock ratio. Longer run length time means decoking less frequently and a longer furnace life span. The utility cost does not significantly affect the overall optimization because utility cost amounts about 4-5% of the gross profits. That also indicates why plant-wide optimization and sub-unit optimization give similar results. The furnace is the critical part of the whole plant and the furnace model sets the overall plant yield and determines the major profit source. Therefore, the furnace is always pushed to operate under its upper limit of the feedstock flow rate to get the maximum profit. This indicates that further improvement in the objective can be obtained by relaxing these constraints in the furnace part through minor capital improvement, e.g., the equipment replacement. However, this was excluded from the current study.

Table 5.5 lists the main products' flow rates and their compositions in the pyrolysis gas for both base case and optimization result while Table 5.6 lists the economic analysis of each final product from the separation system. The extra 6% increase in the gross profit mainly comes from the increased flow rate of propylene, another profitable final product, and the increased run-length time. Figure 5.2 shows the comparison between the mole flow rate of the final product of hydrogen, methane, ethylene, ethane, propylene, and propane. Note that the selectivity of the feedstock is slightly decreased.

Table 5.5. Pyrolysis gas flow rate and its composition (mole%).

Pyrolysis Gas	Base Case (flow rate)	Base Case (mole%)	Optimization (flow rate)	Optimization (mole%)
H ₂	2.736	30.30	2.597	28.21
CH ₄	1.919	21.25	1.717	18.65
C ₂ H ₄	3.015	33.39	2.870	31.17
C ₂ H ₆	0.622	7.33	1.127	12.24
C ₃ H ₆	0.297	3.29	0.444	4.82
C ₃ H ₈	0.082	0.91	0.205	2.22

Table 5.6. Economical analysis of each final product.

Flow	Base Case (\$)	Optimization (\$)
C ₂ H ₄	2.5167	2.3977
C ₂ H ₆ product	0.1547	0.2619
C ₃ H ₆	0.2062	0.3083
C ₃ H ₈ product	0.0347	0.0863
C ₄ ⁺	0.3184	0.3944
C ₅ ⁺	0.1243	0.1023
C ₂ H ₆ feed	0.6596	0.7017
C ₃ H ₈ feed	0.9386	0.9986
fresh C ₂ H ₆ feed	0.5048	0.4399
fresh C ₃ H ₈ feed	0.9039	0.9123

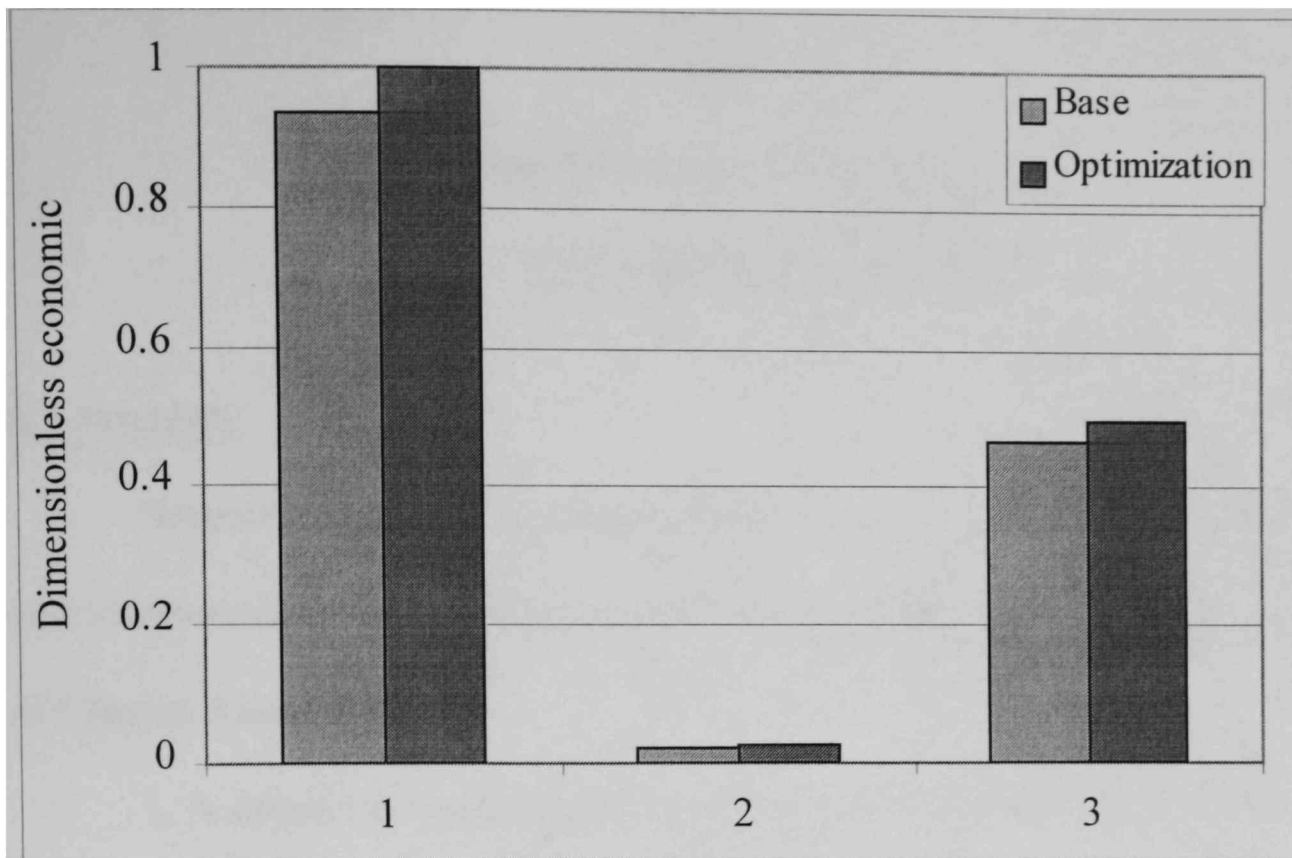


Figure 5.1. Economic comparison between base case and optimization result.

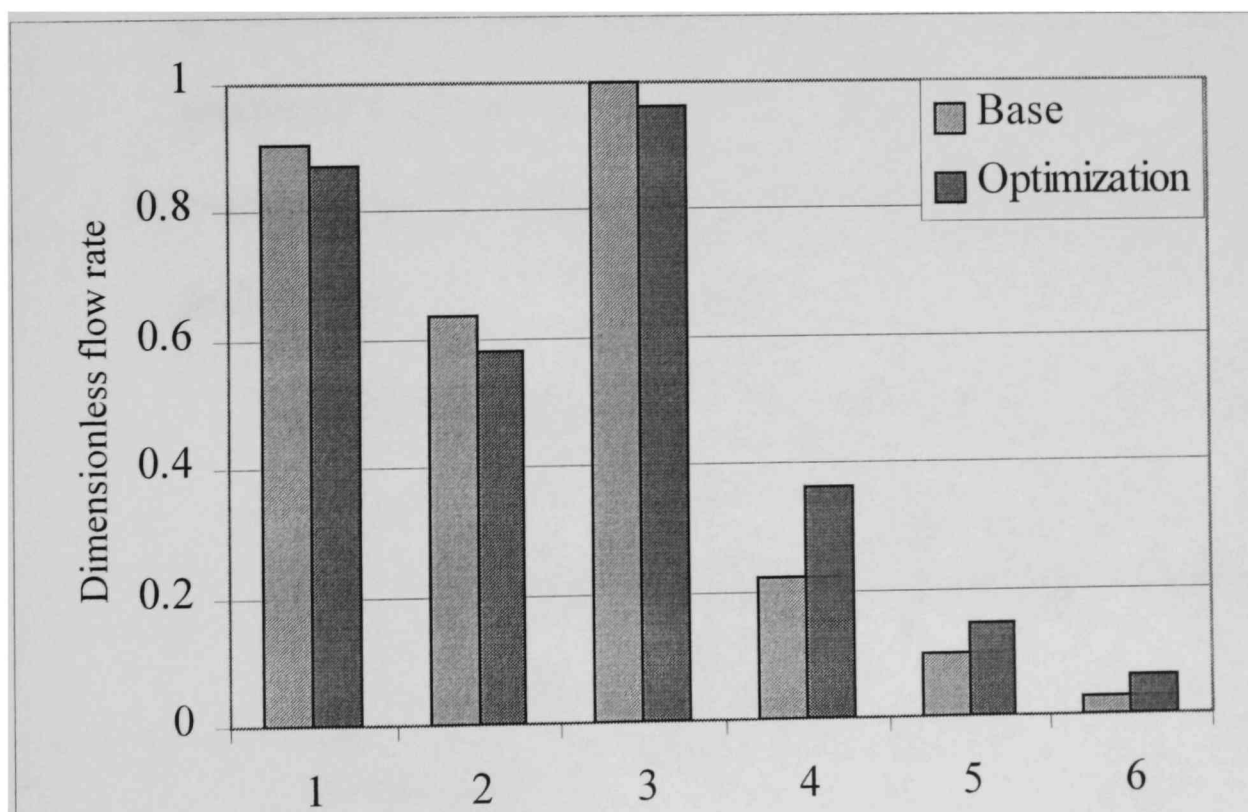


Figure 5.2. Flow rate comparison between base case and optimization results.

CHAPTER 6

DISCUSSION, CONCLUSION AND RECOMMENDATION

6.1 Summary

Several conclusions have been drawn according to the modeling and the optimization study, while the detailed discussions about their results are given at the ends of Chapter 3 and Chapter 5.

1. A simplified furnace model was developed and benchmarked against industrial data of the tube outlet flow and run-length.
2. The short-cut method is employed in the separation system model and gives good predictions on the final product flow, and its corresponding refrigerant requirement and the utility usage.
3. Average prices are used to study this plant-wide time-domain optimization. The findings are:
 - a. The furnace is the critical part of the plant-wide optimization.
 - b. The plant-wide optimization study gives a same answer to the furnace sub-unit optimization study, while the constraints of the separation system and the refrigeration system will limit the maximum feedstock for the furnace.
 - c. By driving the feedstock flow rate to its upper limit and adjusting the dilution steam usage, the whole tube run-length can be increased, as

well as the final plant-wide gross profit, in the preliminary optimization study.

6.2 Recommendations

During more than two years of thorough research on this project, new ideas about the future research directions keep emerging. Some of them may be too ambitious and some of them may be immature. It would please me if the following suggestions could give the graduate student who continues this project some illumination.

1. Convert to open equation-based model

It is highly recommended to convert the sequential model to the open equation-based model because of the unique advantage open equation model. For open equation model, solutions of the equations are not dependent on a specific solution algorithm. In addition, the equations are easier to maintain since they are ordered independently. Also, the same equation could be used for both the parameter fitting and optimization cases. The faster problem solving ability especially benefits recycling process simulation, which is common in the refrigeration system and the cracking product reuse. The benefits of the open-equation format of the RTO model include reduced model development time, easy maintenance, and complete flexibility.

2. Add fire-box model

In my thesis, the heat transfer simulation is simplified by the parameterization. The tube outlet temperature is used to estimate the effective heat load transferred into the cracking tube, which is also assumed to be homogeneous along the tube.

In a real plant, different furnace firing styles have different heat transfer profiles for the reactor. Plehiers, Reyniers and Froment (1990) simulate the heterogeneous heat flux profile based on the external tube surface by the fire box modeling. Paules and Meixell (1994) also indicate that a wall-fired furnace will have a horizontal temperature vs. coil length profile while a floor-fired furnace will have a profile that falls from the furnace floor to the bridgewall. A reactor and coking simulation model coupled with a radiant heat transfer model will give a better prediction in the furnace outlet flow.

3. Increase the flexibility of the cracking model

E/P feed is the common feedstock in the USA now and will occupy a large quantity in the future furnace feedstock market. However, the feedstock for a modern ethylene plant could vary from heavy hydrocarbons to crude oil fraction. Also, from the prices listed in Table 5.2, feedstock price can have a double change within six months which indicates that the plant will have to switch from one feedstock to another according the market demand and supply. Generally, the ethylene plant cracks more vapor light hydrocarbons in the summer time, while cracking more liquid heavy hydrocarbons in winter. It will be more feasible to use a more flexible cracking model in the future plant-wide optimization study to decide which feedstock to buy or how much of each feedstock should be bought if several furnaces are cracking simultaneously.

4. Re-parameterize kinetic data

Since the furnace is the heart of the plant, a more accurate cracking model to predict the pyrolysis effluent flow and conditions is more significant for the

overall simulation and optimization. The measurements of pyrolysis gas compositions are used to periodically online update the kinetic data of the yield model. This periodically updated furnace model can give a better prediction for the cracking effluent and more accurate optimization results.

5. Use stage-to-stage distillation column simulation

The short-cut method gives satisfactory predictions on the heat duty requirement for each distillation column. Olefins plants are highly interactive in nature. The amount of refrigeration required is dependent on the tower operating pressure, the feed rate and composition, and the target product quality. Therefore, a stage-to-stage distillation column model will give better predictions.

6. Use detailed compressor simulation

Stage-by-stage calculations for the compressors are recommended once the compressor performance curve is available. The compressors in the ethylene plant usually limit the maximum pyrolysis gas flow. The compressor suction pressure is very important in the simulation. A detailed compressor simulation is very helpful to check whether the compressors are operated in the normal operation region.

7. Use tiered price model

The average prices are used for the profit objective function. In chemical industrial business, one product may have several different values according to its quantity and quality. From the information of *Chemical Market Reporter*, there could be a one to three cent difference between the chemical grade propylene and the analytic grade propylene. A tiered price model by the market supply and

demand will give an enhanced understanding about the economic issues in the optimization.

BIBLIOGRAPHY

- Albright L.F., B.L. Crynes, and W. H. Corcoran, *Pyrolysis: Theory and Industrial Practice*, Academic Press, Inc., New York, 1983
- Bartusiak R.D., and D.H. Nicholson, "Realtime optimization at the Fife ethylene plant," *Ethylene Producers Conference Proceedings, AIChE*, p.542-556, New York, 1992
- Bennett C.O., and J.E. Myers, *Momentum, Heat, and Mass Transfer*, 2nd ed., McGraw-Hill, New York, 1974
- Chang T., "Worldwide ethylene capacity grows in spite of warning," *Oil and Gas Journal*, p.40-47, Mar. 30, 1998
- Chemical Market Reporter*, New York Schnell Pub. Co., New York, Jan.-Sep., 1999
- Colmenares T. R., and W.D. Seider, "Synthesis of cascade refrigeration systems integrated with chemical processes," *Computers Chem. Engng.*, Vol. 13, No. 3, p.247-258, 1989
- Dente M., E. Ranzi, and A.G. Goossens, "Detailed prediction of olefin yields from hydrocarbon pyrolysis through a fundamental simulation model (SPYRO)," *Computers & Chemical Engineering*, Vol. 3, p.61-75, 1979
- Douglas, J.M., A. Jafarey, and R. Seemann, "Short-cut techniques for distillation column design and control. 2. Column operability and control," *Ind. Eng. Chem. Proc. Des. Dev.*, Vol. 18, No. 2, p.203-210, 1979
- Fatora C.F., S.L. Davenport, and D.N. Kelly, "Implementation of a closed loop real-time optimization system on a large scale ethylene plant," *Advances in Instrumentation and Control: Proceedings of the ISA, International Conference and Exhibit*, Vol. 46, Part 1, p.841-852, 1991
- Frank C.F., G.B. Gochenour, and D.N. Kelly, "Modeling ethylene plants for real-time optimization applications," *AIChE Spring National Meeting / Industrial Applications of Process Control*, April 1992
- Georgiou A., A.V. Sapre, P. Taylor, R.E. Galloway, and L.K. Casey, "Ethylene optimization system reaps operations and maintenance benefits," *Oil and Gas Journal*, Mar. 9, p.46-50, 1998

- Gill P.E., W. Murray, M.A. Saunders, and M.H. Wright, *User's Guide for NPSOL (Version 4.0): a Fortran Package for Nonlinear Programming*. Report SOL 86-2. Systems Optimization Laboratory, Stanford University, 1986
- Heynderickx G.J., and G.F. Froment, "Simulation and comparison of the run length of an ethane cracking furnace with reactor tubes of circular and elliptical cross sections," *Ind. Eng. Chem. Res.*, No. 37, p.914-922, 1998
- Huang S., and H. Shao, "Application of pattern recognition to ethylene production optimization," *Engng Applic. Artif. Intell.*, Vol. 7, No.3, p.329-333, 1994
- Hurstel V., P. Lepetit, and V. Kaiser, "Refrigeration schemes serve olefin plant needs." *Oil and Gas Journal*, p.107-123, Sep 7, 1981
- Jafarey A., J. M. Douglas, and T. J. McAvoy, "Short-cut techniques for distillation column design and control. 1. Column design," *Ind. Eng. Chem. Proc. Des. Dev.*, Vol. 18, No.2, P.197-202, 1979
- Kelly D.N., F.C. Fatora, and S.L. Davenport, "Implementaion of a closed loop real time optimization system on a large scale ethylene plant," *Meeting of the Instrument Society of America*, Anaheim, Cal., Oct. 1991
- Kister H.Z., *Distillation Design*, McGraw-Hill Inc., New York, 1992
- Kniel L., O. Winter, and K. Stork, *Ethylene, Key Stone to the Petrochemical Industry*, Marcel Dekker, Inc., New York, 1980
- Lauks U.E., R.J. Vasbinder, P.J. Valkenburg, and C. Van Leeuwen, "On-line optimization of an ethylene plant," *Computers & chemical engineering, European Symposium On Computer Aided Process Engineering—1*, Vol. 16, S213, May 1992
- Office of Chemicals and Allied Products Basic Industries, *A Competitive Assessment of the US Ethylene Industry*, U.S. Department of Commerce, International Trade Administration, Washington D.C., Dec. 1986
- Paules G.E. IV, and M.D. Meixell Jr., "A fundamental free radical kinetic pyrolysis model for on-line, closed-loop plant-wide optimization of olefins plants," *CIMPRO '94*, New Brunswick, NJ, April 25, 1994
- Plehiers P.M., G.C. Reyniers, and G.F. Froment, "Simulation of the run length of an ethane cracking furnace," *Ind. Eng. Chem. Res.*, No. 29, p.636-641, 1990
- Reid R.C., J.M. Prausnitz, and B.E. Poling, *The Properties of Gases and Liquids*, 4th ed., McGraw-Hill Book Company, New York, 1987

- Riggs J.B., *An Introduction to Numerical Methods for Chemical Engineers*, 2nd Ed., Texas Tech University Press, Lubbock, Texas, 1994
- Smith B.D., and W.K. Brinkley, "General short-cut equation for equilibrium stage processes," *AIChE Journal*, p.446-450, Sep. 1960
- Smoker E.J., "Analytic determination of plates in fractionating columns," *Trans. Am., Inst. Chem. Engrs.*, Vol. 34, p.165, 1938
- Sourander M.L., M. Lolari, J.C. Cugini, J.B. Poje, and D.C. White, "Control and optimization of olefin-cracking heaters," *Hydrocarbon Processing*, p.63-69, June 1984
- Sundaram K.M., and G.F. Froment, "Modeling of thermal cracking kinetics, 3. Radical Mechanisms for the pyrolysis of simple paraffins, olefins and their mixtures," *Ind. Eng. Chem. Fundam.*, Vol. 17, No. 3, p.174-182, 1978
- Sundaram K.M., and G.F. Froment, "Kinetics of coke deposition in the thermal cracking of propane," *Chemical Engineering Science*, Vol. 34, p.635-644, 1979
- Sundaram K.M., P.S. Vandamme, and G.F. Froment, "Coke deposition in the thermal cracking of ethane," *AIChE Journal*, Vol. 27, No. 6, p.946-951, Nov. 1981
- Tsai T.C., R. Zou, and J. Zou, "Model predicts yields from ethane-propane cocracking," *Oil and Gas Journal*, p.38-41, Dec 21, 1987

APPENDIX A

THE REACTION NETWORK FOR E/P FEED

(Sundaram and Froment, 1978)

Table A.1. Reaction network and its kinetic data.

No	Reaction	A (kcal/mole)	E (sec^{-1} or $\text{L}/\text{mole}\cdot\text{sec}$)	Reaction Rate
1	$\text{C}_2\text{H}_6 \rightarrow 2\text{CH}_3\bullet$	4.0×10^{16}	87.5	$r_1 = k_1[\text{C}_2\text{H}_6]$
2	$\text{C}_3\text{H}_8 \rightarrow \text{C}_2\text{H}_5\bullet + \text{CH}_3\bullet$	2.0×10^{16}	84.5	$r_2 = k_2[\text{C}_3\text{H}_8]$
3	$\text{n-C}_4\text{H}_{10} \rightarrow 2\text{C}_2\text{H}_5\bullet$	1.5×10^{16}	82.1	$r_3 = k_3[\text{n-C}_4\text{H}_{10}]$
4	$\text{n-C}_4\text{H}_{10} \rightarrow \text{1-C}_3\text{H}_7\bullet + \text{CH}_3\bullet$	9.0×10^{16}	85.4	$r_4 = k_4[\text{n-C}_4\text{H}_{10}]$
5	$\text{1-C}_4\text{H}_8 \rightarrow \text{C}_3\text{H}_5\bullet + \text{CH}_3\bullet$	8.0×10^{16}	74.0	$r_5 = k_5[\text{1-C}_4\text{H}_8]$
6	$\text{C}_2\text{H}_4 + \text{H}\bullet \rightarrow \text{C}_2\text{H}_3\bullet + \text{H}_2$	8.0×10^8	4.0	$r_6 = k_6[\text{C}_2\text{H}_4][\text{H}\bullet]$
7	$\text{C}_2\text{H}_6 + \text{H}\bullet \rightarrow \text{C}_2\text{H}_5\bullet + \text{H}_2$	1.0×10^{11}	9.7	$r_7 = k_7[\text{C}_2\text{H}_6][\text{H}\bullet]$
8	$\text{C}_3\text{H}_6 + \text{H}\bullet \rightarrow \text{C}_3\text{H}_5\bullet + \text{H}_2$	2.5×10^9	1.1	$r_8 = k_8[\text{C}_3\text{H}_6][\text{H}\bullet]$
9	$\text{C}_3\text{H}_8 + \text{H}\bullet \rightarrow \text{1-C}_3\text{H}_7\bullet + \text{H}_2$	1.0×10^{11}	9.7	$r_9 = k_9[\text{C}_3\text{H}_8][\text{H}\bullet]$
10	$\text{C}_3\text{H}_8 + \text{H}\bullet \rightarrow 2\text{-C}_3\text{H}_7\bullet + \text{H}_2$	9.0×10^{10}	8.3	$r_{10} = k_{10}[\text{C}_3\text{H}_8][\text{H}\bullet]$
11	$\text{1-C}_4\text{H}_8 + \text{H}\bullet \rightarrow \text{C}_4\text{H}_7\bullet + \text{H}_2$	5.0×10^{10}	3.9	$r_{11} = k_{11}[\text{1-C}_4\text{H}_8][\text{H}\bullet]$
12	$\text{C}_2\text{H}_4 + \text{CH}_3\bullet \rightarrow \text{C}_2\text{H}_3\bullet + \text{CH}_4$	1.0×10^{10}	13.0	$r_{12} = k_{12}[\text{C}_2\text{H}_4][\text{CH}_3\bullet]$
13	$\text{C}_2\text{H}_6 + \text{CH}_3\bullet \rightarrow \text{C}_2\text{H}_5\bullet + \text{CH}_4$	3.8×10^{11}	16.5	$r_{13} = k_{13}[\text{C}_2\text{H}_6][\text{CH}_3\bullet]$
14	$\text{C}_3\text{H}_6 + \text{CH}_3\bullet \rightarrow \text{C}_3\text{H}_5\bullet + \text{CH}_4$	2.0×10^9	12.2	$r_{14} = k_{14}[\text{C}_3\text{H}_6][\text{CH}_3\bullet]$

Table A.1. Continued

No	Reaction	A ($kcal/mole$)	E (sec^{-1} or $L/mole \cdot sec$)	Reaction Rate
16	$C_3H_8 + CH_3\bullet \rightarrow 2-C_3H_7\bullet + CH_4$	4.0×10^9	10.1	$r_{16} = k_{16} [C_3H_8] [CH_3\bullet]$
17	$1-C_4H_8 + CH_3\bullet \rightarrow C_4H_7\bullet + CH_4$	1.0×10^8	7.3	$r_{17} = k_{17} [1-C_4H_8] [CH_3\bullet]$
18	$C_3H_6 + C_2H_3\bullet \rightarrow C_3H_5\bullet + C_2H_4$	3.0×10^9	14.5	$r_{18} = k_{18} [C_3H_6] [C_2H_3\bullet]$
19	$C_3H_8 + C_2H_3\bullet \rightarrow 1-C_3H_7\bullet + C_2H_4$	3.0×10^9	18.8	$r_{19} = k_{19} [C_3H_8] [C_2H_3\bullet]$
20	$C_3H_8 + C_2H_3\bullet \rightarrow 2-C_3H_7\bullet + C_2H_4$	1.0×10^9	16.2	$r_{20} = k_{20} [C_3H_8] [C_2H_3\bullet]$
21	$C_2H_4 + C_2H_5\bullet \rightarrow CH_3\bullet + C_3H_6$	3.0×10^9	19.0	$r_{21} = k_{21} [C_2H_4] [C_2H_5\bullet]$
22	$C_3H_6 + C_2H_5\bullet \rightarrow C_3H_5\bullet + C_2H_6$	1.0×10^8	9.2	$r_{22} = k_{22} [C_3H_6] [C_2H_5\bullet]$
23	$C_3H_8 + C_2H_5\bullet \rightarrow 1-C_3H_7\bullet + C_2H_6$	1.2×10^9	12.6	$r_{23} = k_{23} [C_3H_8] [C_2H_5\bullet]$
24	$C_3H_8 + C_2H_5\bullet \rightarrow 2-C_3H_7\bullet + C_2H_6$	8.0×10^8	10.4	$r_{24} = k_{24} [C_3H_8] [C_2H_5\bullet]$
25	$C_3H_8 + C_3H_5\bullet \rightarrow 1-C_3H_7\bullet + C_3H_6$	1.0×10^9	18.8	$r_{25} = k_{25} [C_3H_8] [C_3H_5\bullet]$
26	$C_3H_8 + C_3H_5\bullet \rightarrow 2-C_3H_7\bullet + C_3H_6$	8.0×10^8	16.2	$r_{26} = k_{26} [C_3H_8] [C_3H_5\bullet]$
27	$C_2H_3\bullet \rightarrow C_2H_2 + H\bullet$	2.0×10^9	31.5	$r_{27} = k_{27} [C_2H_3\bullet]$
28	$C_2H_5\bullet \rightarrow C_2H_4 + H\bullet$	3.2×10^{13}	40.0	$r_{28} = k_{28} [C_2H_5\bullet]$
29	$C_3H_5\bullet \rightarrow C_2H_2 + CH_3\bullet$	3.0×10^{10}	36.2	$r_{29} = k_{29} [C_3H_5\bullet]$
30	$1-C_3H_7\bullet \rightarrow C_2H_4 + CH_3\bullet$	4.0×10^{13}	32.6	$r_{30} = k_{30} [1-C_3H_7\bullet]$
31	$1-C_3H_7\bullet \rightarrow C_3H_6 + H\bullet$	2.0×10^{13}	34.8	$r_{31} = k_{31} [1-C_3H_7\bullet]$

Table A.1. Continued

No	Reaction	A ($kcal/mole$)	E (sec^{-1} or $L/mole \cdot sec$)	Reaction Rate
33	$C_4H_7\bullet \rightarrow C_4H_6 + H\bullet$	1.2×10^{14}	49.3	$r_{33} = k_{33} [C_4H_7\bullet]$
34	$C_4H_7\bullet \rightarrow C_2H_4 + C_2H_3\bullet$	1.0×10^{11}	37.0	$r_{34} = k_{34} [C_4H_7\bullet]$
35	$1-C_4H_9\bullet \rightarrow C_2H_4 + C_2H_5\bullet$	1.6×10^{12}	28.0	$r_{35} = k_{35} [1-C_4H_9\bullet]$
36	$1-C_4H_9\bullet \rightarrow 1-C_4H_8 + H\bullet$	1.0×10^{13}	36.6	$r_{36} = k_{36} [1-C_4H_9\bullet]$
37	$2-C_4H_9\bullet \rightarrow C_3H_6 + CH_3\bullet$	2.5×10^{13}	31.9	$r_{37} = k_{37} [2-C_4H_9\bullet]$
38	$2-C_4H_9\bullet \rightarrow 1-C_4H_8 + H\bullet$	2.0×10^{13}	39.8	$r_{38} = k_{38} [2-C_4H_9\bullet]$
39	$C_5H_{11}\bullet \rightarrow C_5H_{10} + H\bullet$	5.0×10^{13}	36.6	$r_{39} = k_{39} [C_5H_{11}\bullet]$
40	$C_5H_{11}\bullet \rightarrow 1-C_4H_8 + CH_3\bullet$	3.2×10^{13}	31.5	$r_{40} = k_{40} [C_5H_{11}\bullet]$
41	$C_5H_{11}\bullet \rightarrow C_2H_4 + 1-C_3H_7\bullet$	4.0×10^{12}	28.7	$r_{41} = k_{41} [C_5H_{11}\bullet]$
42	$C_2H_2 + H\bullet \rightarrow C_2H_3\bullet$	4.0×10^{10}	1.3	$r_{42} = k_{42} [C_2H_2][H\bullet]$
43	$C_2H_4 + H\bullet \rightarrow C_2H_5\bullet$	1.0×10^{10}	1.5	$r_{43} = k_{43} [C_2H_4][H\bullet]$
44	$C_3H_6 + H\bullet \rightarrow 1-C_3H_7\bullet$	1.0×10^{10}	2.9	$r_{44} = k_{44} [C_3H_6][H\bullet]$
45	$C_3H_6 + H\bullet \rightarrow 2-C_3H_7\bullet$	1.0×10^{10}	1.5	$r_{45} = k_{45} [C_3H_6][H\bullet]$
46	$C_4H_6 + H\bullet \rightarrow C_4H_7\bullet$	4.0×10^{10}	1.3	$r_{46} = k_{46} [C_4H_6][H\bullet]$
47	$1-C_4H_8 + H\bullet \rightarrow 2-C_4H_9\bullet$	1.0×10^{10}	1.2	$r_{47} = k_{47} [1-C_4H_8][H\bullet]$
48	$C_2H_4 + CH_3\bullet \rightarrow 1-C_3H_7\bullet$	2.0×10^8	7.9	$r_{48} = k_{48} [C_2H_4][CH_3\bullet]$

Table A.1. Continued

No	Reaction	A ($kcal/mole$)	E (sec^{-1} or $L/mole \cdot sec$)	Reaction Rate
50	$C_2H_4 + C_2H_3\bullet \rightarrow C_4H_7\bullet$	5.0×10^7	7.0	$r_{50} = k_{50}[C_2H_4][C_2H_3\bullet]$
51	$C_2H_4 + C_2H_5\bullet \rightarrow 1-C_4H_9\bullet$	1.5×10^7	7.6	$r_{51} = k_{51}[C_2H_4][C_2H_5\bullet]$
52	$C_3H_6 + C_2H_5\bullet \rightarrow C_5H_{11}\bullet$	1.3×10^7	7.5	$r_{52} = k_{52}[C_3H_6][C_2H_5\bullet]$
53	$C_2H_4 + 1-C_3H_7\bullet \rightarrow C_5H_{11}\bullet$	2.0×10^7	7.4	$r_{53} = k_{53}[C_2H_4][1-C_3H_7\bullet]$
54	$C_2H_4 + 2-C_3H_7\bullet \rightarrow C_5H_{11}\bullet$	1.3×10^7	6.9	$r_{54} = k_{54}[C_2H_4][2-C_3H_7\bullet]$
55	$1-C_4H_9\bullet \rightarrow 2-C_4H_9\bullet$	5.2×10^{14}	41.0	$r_{55} = k_{55}[1-C_4H_9\bullet]$
56	$C_2H_3\bullet + H\bullet \rightarrow C_2H_4$	1.0×10^{10}	0	$r_{56} = k_{56}[C_2H_3\bullet][H\bullet]$
57	$C_2H_5\bullet + H\bullet \rightarrow C_2H_6$	4.0×10^{10}	0	$r_{57} = k_{57}[C_2H_5\bullet][H\bullet]$
58	$C_3H_5\bullet + H\bullet \rightarrow C_3H_6$	2.0×10^{10}	0	$r_{58} = k_{58}[C_3H_5\bullet][H\bullet]$
59	$1-C_3H_7\bullet + H\bullet \rightarrow C_3H_8$	1.0×10^{10}	0	$r_{59} = k_{59}[1-C_3H_7\bullet][H\bullet]$
60	$2-C_3H_7\bullet + H\bullet \rightarrow C_3H_8$	1.0×10^{10}	0	$r_{60} = k_{60}[2-C_3H_7\bullet][H\bullet]$
61	$C_4H_7\bullet + H\bullet \rightarrow 1-C_4H_8$	2.0×10^{10}	0	$r_{61} = k_{61}[C_4H_7\bullet][H\bullet]$
62	$1-C_4H_9\bullet + H\bullet \rightarrow n-C_4H_{10}$	1.0×10^{10}	0	$r_{62} = k_{62}[1-C_4H_9\bullet][H\bullet]$
63	$2-C_4H_9\bullet + H\bullet \rightarrow n-C_4H_{10}$	1.0×10^{10}	0	$r_{63} = k_{63}[2-C_4H_9\bullet][H\bullet]$
64	$C_5H_{11}\bullet + H\bullet \rightarrow C_5H_{12}$	1.0×10^{10}	0	$r_{64} = k_{64}[C_5H_{11}\bullet][H\bullet]$
65	$CH_3\bullet + CH_3\bullet \rightarrow C_2H_6$	1.3×10^{10}	0	$r_{65} = k_{65}[CH_3\bullet][CH_3\bullet]$

Table A.1 Continued

No	Reaction	A (kcal/mole)	E (sec^{-1} or $\text{L}/\text{mole} \cdot \text{sec}$)	Reaction Rate
67	$\text{C}_3\text{H}_5\bullet + \text{CH}_3\bullet \rightarrow 1\text{-C}_4\text{H}_8$	3.2×10^9	0	$r_{67} = k_{67}[\text{C}_3\text{H}_5\bullet][\text{CH}_3\bullet]$
68	$1\text{-C}_3\text{H}_7\bullet + \text{CH}_3\bullet \rightarrow n\text{-C}_4\text{H}_{10}$	3.2×10^9	0	$r_{68} = k_{68}[1\text{-C}_3\text{H}_7\bullet][\text{CH}_3\bullet]$
69	$2\text{-C}_3\text{H}_7\bullet + \text{CH}_3\bullet \rightarrow n\text{-C}_4\text{H}_{10}$	3.2×10^9	0	$r_{69} = k_{69}[2\text{-C}_3\text{H}_7\bullet][\text{CH}_3\bullet]$
70	$\text{C}_4\text{H}_7\bullet + \text{CH}_3\bullet \rightarrow \text{C}_5^+$	3.2×10^9	0	$r_{70} = k_{70}[\text{C}_4\text{H}_7\bullet][\text{CH}_3\bullet]$
71	$\text{C}_2\text{H}_3\bullet + \text{C}_2\text{H}_3\bullet \rightarrow \text{C}_4\text{H}_6$	1.3×10^{10}	0	$r_{71} = k_{71}[\text{C}_2\text{H}_3\bullet][\text{C}_2\text{H}_3\bullet]$
72	$\text{C}_4\text{H}_7\bullet + \text{C}_2\text{H}_3\bullet \rightarrow \text{C}_5^+$	1.3×10^{10}	0	$r_{72} = k_{72}[\text{C}_4\text{H}_7\bullet][\text{C}_2\text{H}_3\bullet]$
73	$\text{C}_2\text{H}_5\bullet + \text{C}_2\text{H}_5\bullet \rightarrow n\text{-C}_4\text{H}_{10}$	4.0×10^8	0	$r_{73} = k_{73}[\text{C}_2\text{H}_5\bullet][\text{C}_2\text{H}_5\bullet]$
74	$\text{C}_2\text{H}_5\bullet + \text{C}_2\text{H}_5\bullet \rightarrow \text{C}_2\text{H}_4 + \text{C}_2\text{H}_6$	5.0×10^7	0	$r_{74} = k_{74}[\text{C}_2\text{H}_5\bullet][\text{C}_2\text{H}_5\bullet]$
75	$\text{C}_3\text{H}_5\bullet + \text{C}_2\text{H}_5\bullet \rightarrow \text{C}_5^+$	3.2×10^9	0	$r_{75} = k_{75}[\text{C}_3\text{H}_5\bullet][\text{C}_2\text{H}_5\bullet]$
76	$1\text{-C}_3\text{H}_7\bullet + \text{C}_2\text{H}_5\bullet \rightarrow \text{C}_5^+$	8.0×10^8	0	$r_{76} = k_{76}[1\text{-C}_3\text{H}_7\bullet][\text{C}_2\text{H}_5\bullet]$
77	$2\text{-C}_3\text{H}_7\bullet + \text{C}_2\text{H}_5\bullet \rightarrow \text{C}_5^+$	8.0×10^8	0	$r_{77} = k_{77}[2\text{-C}_3\text{H}_7\bullet][\text{C}_2\text{H}_5\bullet]$
78	$\text{C}_4\text{H}_7\bullet + \text{C}_2\text{H}_5\bullet \rightarrow \text{C}_5^+$	3.2×10^9	0	$r_{78} = k_{78}[\text{C}_4\text{H}_7\bullet][\text{C}_2\text{H}_5\bullet]$
79	$\text{C}_3\text{H}_5\bullet + \text{C}_3\text{H}_5\bullet \rightarrow \text{C}_5^+$	3.2×10^9	0	$r_{79} = k_{79}[\text{C}_3\text{H}_5\bullet][\text{C}_3\text{H}_5\bullet]$
80	$\text{C}_4\text{H}_7\bullet + \text{C}_3\text{H}_5\bullet \rightarrow \text{C}_5^+$	1.3×10^{10}	0	$r_{80} = k_{80}[\text{C}_4\text{H}_7\bullet][\text{C}_3\text{H}_5\bullet]$
81	$\text{C}_4\text{H}_7\bullet + \text{C}_4\text{H}_7\bullet \rightarrow \text{C}_5^+$	3.2×10^9	0	$r_{81} = k_{81}[\text{C}_4\text{H}_7\bullet][\text{C}_4\text{H}_7\bullet]$
82	$\text{C}_2\text{H}_2 \rightarrow 2\text{C} + \text{H}_2$	5.0×10^{12}	62.0	$r_{82} = k_{82}[\text{C}_2\text{H}_2]$

Table A.2. Components list and their related reactions.

No.	Species	Related Reaction	No. of Total Reactions
1	H ₂	$r_6 + r_7 + r_8 + r_9 + r_{10} + r_{11} + r_{82}$	7
2	CH ₄	$r_{12} + r_{13} + r_{14} + r_{15} + r_{16} + r_{17}$	6
3	C ₂ H ₂	$r_{27} + r_{29} - r_{42} - r_{82}$	4
4	C ₂ H ₄	$-r_6 - r_{12} + r_{18} + r_{19} + r_{20} - r_{21} + r_{28} + r_{30} + r_{34} + r_{35} + r_{41} - r_{43} - r_{48} - r_{50} - r_{51} - r_{53} - r_{54} + r_{56} + r_{74}$	19
5	C ₂ H ₆	$-r_1 - r_7 - r_{13} + r_{22} + r_{23} + r_{24} + r_{57} + r_{65} + r_{74}$	9
6	C ₃ H ₆	$-r_8 - r_{14} - r_{18} + r_{21} - r_{22} + r_{25} + r_{26} + r_{31} + r_{32} + r_{37} - r_{44} - r_{45} - r_{49} - r_{52} + r_{58}$	15
7	C ₃ H ₈	$-r_2 - r_9 - r_{10} - r_{15} - r_{16} - r_{19} - r_{20} - r_{23} - r_{24} - r_{25} - r_{26} + r_{59} + r_{60} + r_{66}$	14
8	C ₄ H ₆	$r_{33} - r_{46} + r_{71}$	3
9	1-C ₄ H ₈	$-r_5 - r_{11} - r_{17} + r_{36} + r_{38} + r_{40} - r_{47} + r_{61} + r_{67}$	9
10	n-C ₄ H ₁₀	$-r_3 - r_4 + r_{62} + r_{63} + r_{68} + r_{68} + r_{73}$	7
11	C ₅ ⁺	$r_{39} + r_{64} + r_{70} + r_{72} + r_{75} + r_{76} + r_{77} + r_{78} + r_{79} + r_{80} + r_{81}$	11

Table A.3. Free radicals list and their related reactions.

No.	Species	Related Reaction	No. of Total Reactions
12	H•	-r ₆ -r ₇ -r ₈ -r ₉ -r ₁₀ -r ₁₁ +r ₂₇ +r ₂₈ +r ₃₁ +r ₃₂ +r ₃₃ +r ₃₆ +r ₃₈ +r ₃₉ -r ₄₂ -r ₄₃ -r ₄₄ -r ₄₅ -r ₄₆ -r ₄₇ -r ₅₆ -r ₅₇ -r ₅₈ -r ₅₉ -r ₆₀ -r ₆₁ -r ₆₂ -r ₆₃ -r ₆₄	29
13	CH ₃ •	2r ₁ +r ₂ +r ₄ +r ₅ -r ₁₂ -r ₁₃ -r ₁₄ -r ₁₅ -r ₁₆ -r ₁₇ +r ₂₁ +r ₂₉ +r ₃₀ +r ₃₇ +r ₄₀ -r ₄₈ -r ₄₉ -2r ₆₅ -r ₆₆ -r ₆₇ -r ₆₈ -r ₆₉ -r ₇₀	23
14	C ₂ H ₃ •	r ₆ +r ₁₂ -r ₁₈ -r ₁₉ -r ₂₀ -r ₂₇ +r ₃₄ +r ₄₂ -r ₅₀ -r ₅₆ -2r ₇₁ -r ₇₂	12
15	C ₂ H ₅ •	r ₂ +2r ₃ +r ₇ +r ₁₃ -r ₂₁ -r ₂₂ -r ₂₃ -r ₂₄ -r ₂₈ +r ₃₅ +r ₄₃ -r ₅₁ -r ₅₂ -r ₅₇ -r ₆₆ -2r ₇₃ -2r ₇₄ -r ₇₅ -r ₇₆ -r ₇₇ -r ₇₈	21
16	C ₃ H ₅ •	r ₅ +r ₈ +r ₁₄ +r ₁₈ +r ₂₂ -r ₂₅ -r ₂₆ -r ₂₉ -r ₅₈ -r ₆₇ -r ₇₅ -2r ₇₉ -r ₈₀	13
17	1-C ₃ H ₇ •	r ₄ +r ₉ +r ₁₅ +r ₁₉ +r ₂₃ +r ₂₅ -r ₃₀ -r ₃₁ +r ₄₁ +r ₄₄ +r ₄₈ -r ₅₃ -r ₅₉ -r ₆₈ -r ₇₆	15
18	2-C ₃ H ₇ •	r ₁₀ +r ₁₆ +r ₂₀ +r ₂₄ +r ₂₆ -r ₃₂ +r ₄₅ -r ₅₄ -r ₆₀ -r ₆₉ -r ₇₇	11
19	C ₄ H ₇ •	r ₁₁ +r ₁₇ -r ₃₃ -r ₃₄ +r ₄₆ +r ₅₀ -r ₆₁ -r ₇₀ -r ₇₂ -r ₇₈ -r ₈₀ -2r ₈₁	12
20	1-C ₄ H ₉ •	-r ₃₅ -r ₃₆ +r ₄₉ +r ₅₁ -r ₅₅ -r ₆₂	6
21	2-C ₄ H ₉ •	-r ₃₇ -r ₃₈ +r ₄₇ +r ₅₅ -r ₆₃	5
22	C ₅ H ₁₁ •	-r ₃₉ -r ₄₀ -r ₄₁ +r ₅₂ +r ₅₃ +r ₅₄ -r ₆₄	7

APPENDIX B

VISCOSITY OF GAS MIXTURE AT LOW PRESSURE

(Reid et al., 1987)

1. Lucas' correlation equation for low-pressure viscosity of pure gas

$$\eta \cdot \xi = [0.807 \cdot T_r^{0.618} - 0.357 \cdot \exp(-0.449 \cdot T_r) + 0.340 \cdot \exp(-4.058 \cdot T_r) + 0.018] \cdot F_p^\circ \cdot F_Q^\circ$$

$$\xi = 0.176 \cdot \left(\frac{T_c}{M^3 \cdot P_c^4} \right)^{1/6}$$

where

ξ = reduced, inverse viscosity, μP^{-1}

T_c = critical temperature, K

M = molecular weight, $g/mole$

P_c = critical pressure, bars

T_r = reduced temperature

F_p°, F_Q° = correction factors for polarity or quantum effect.

2. Correction factor of F_p°

$$F_p^\circ = 1 \quad 0 \leq \mu_r < 0.022$$

$$F_p^\circ = 1 + 30.55(0.292 - Z_c)^{1.72} \quad 0.022 \leq \mu_r < 0.075$$

$$F_p^\circ = 1 + 30.55(0.292 - Z_c)^{1.72} |0.96 + 0.1(T_r - 0.7)| \quad 0.075 \leq \mu_r$$

where μ_r is defined as:

$$\mu_r = 52.46 \frac{\mu^2 P_c}{T_c^2}.$$

3. Correction Factor F_Q°

F_Q° is only used for the quantum gases He, H₂ and D₂.

$$F_Q^\circ = 1.22 Q^{0.15} \{1 + 0.00385[(T_r - 12)^2]^{1/4} \text{sign}(T_r - 12)\}$$

sign() indicates that one should use +1 or −1 depending on whether the values of the argument () is >0 or <0 .

APPENDIX C

REACTION HEAT CALCULATION

For a reaction like $a \cdot A + b \cdot B \rightarrow c \cdot C + d \cdot D$,

the heat of reaction at temperature T is $\Delta H_R(T) = \Delta H_R^\circ(T_R) + \int_{T_R}^T \Delta C_p dT$,

where $\Delta H_R^\circ(T_R)$ is the heat of the reaction at the reference temperature T_R .

ΔC_p is the overall change in the heat capacity per mole of A reacted.

$$\Delta H_R^\circ(T_R) = \frac{d}{a} \cdot H_D^\circ(T_R) + \frac{c}{a} \cdot H_C^\circ(T_R) - \frac{b}{a} \cdot H_B^\circ(T_R) - H_A^\circ(T_R)$$

$$\Delta C_p = \frac{d}{a} \cdot C_{pD} + \frac{c}{a} \cdot C_{pC} - \frac{b}{a} \cdot C_{pB} - C_{pA}$$

The enthalpy of heat formation of compound i, is usually tabulated at 25°C and can be readily found in *the Properties of Gases & Liquids* and other similar books. The ideal gas isobaric heat capacity is usually expressed by a higher order of polynomial equation with absolute temperature. The equation parameters, which can also be found in such books, are listed in Appendix E.

APPENDIX D

ENTHALPY CALCULATION BY SRK STATE EQUATION

(Soave, 1972)

The enthalpy of a species is

$$H = H^* + \left(\frac{H - H^*}{R \cdot T} \right) \cdot R \cdot T$$

where

H : species enthalpy at temperature T

H^* : the ideal gas state enthalpy at temperature T

$\frac{H - H^*}{R \cdot T}$: enthalpy departure function.

The ideal gas state enthalpy at temperature T is

$$H^* = \Delta H_f^{298.15} + \int_{298.15}^T C_p dT$$

where

$\Delta H_f^{298.15}$: heat of formation of gas at $298.15^\circ K$

C_p : ideal gas heat capacity

$$C_p = a + b \cdot T + c \cdot T^2 + d \cdot T^3.$$

For Soave-Redlich-Kwong state equation model,

$$P = \frac{R \cdot T}{V - b} - \frac{a}{V \cdot (V + b)}$$

and the enthalpy departure function is:

$$\frac{H - H^*}{R \cdot T} = z - 1 - \frac{A}{B} \cdot \left(1 - \frac{T}{a} \cdot \frac{da}{dT}\right) \cdot \ln\left(1 + \frac{B}{Z}\right)$$

where

$$T \cdot \frac{da}{dT} = - \sum_i^N \sum_j^M x_i \cdot x_j \cdot m_j \cdot (ac_i \cdot ac_j \cdot Tr_j)^{0.5} \cdot (1 - k_{ij})$$

$$b = \sum_i^N x_i \cdot b_i$$

$$b_i = 0.08664 \cdot \frac{R \cdot Tc_i}{Pc_i}$$

$$a = \sum_i^N \sum_j^N x_i \cdot x_j \cdot (a_i \cdot a_j)^{0.5} \cdot (1 - k_{ij})$$

$$a_i = ac_i \cdot \alpha_i$$

$$ac_i = 0.42748 \cdot \frac{(R \cdot Tc_i)^2}{Pc_i}$$

$$\alpha_i^{0.5} = 1 + m_i \cdot (1 - Tr_i^{0.5})$$

$$m_i = 0.48 + 1.574 \cdot \omega_i - 0.176 \cdot \omega_i^2$$

$$A = \frac{a \cdot P}{(R \cdot T)^2}$$

$$B = \frac{b \cdot P}{R \cdot T} \cdot$$

APPENDIX E

PHYSICAL PROPERTIES DATA

(Reid, Prausnitz and Poling, 1987)

Table E.1. Component enthalpy of formation and molecular weight.

No.	Species	ΔH_f^* (J/mole)	MW
1	H ₂	0.	2.016
2	CH ₄	-7.490×10^4	16.043
3	C ₂ H ₂	2.269×10^5	26.038
4	C ₂ H ₄	5.234×10^4	28.054
5	C ₂ H ₆	-8.474×10^4	30.070
6	C ₃ H ₆	2.043×10^4	42.081
7	C ₃ H ₈	-1.039×10^5	44.097
8	C ₄ H ₆ ^{**}	1.102×10^5	54.092
9	1-C ₄ H ₈	-1.260×10^2	56.108
10	n-C ₄ H ₁₀	-1.262×10^5	58.124
11	C ₅ ⁺ ^{***}	-1.465×10^5	72.151
12	H•	2.180×10^5	1.016
13	CH ₃ •	1.422×10^5	15.043
14	C ₂ H ₃ •	2.88×10^5	27.054
15	C ₂ H ₅ •	1.088×10^5	29.070
16	C ₃ H ₅ •	2.416×10^5	41.097
17	1-C ₃ H ₇ •	8.70×10^4	43.097
18	2-C ₃ H ₇ •	7.24×10^4	43.097
19	C ₄ H ₇ •	1.285×10^5	55.108
20	1-C ₄ H ₉ •	6.62×10^4	57.124
21	2-C ₄ H ₉ •	5.15×10^4	57.124
22	C ₅ H ₁₁ •	3.73×10^4	71.151
23	H ₂ O	2.018×10^4	18.015

* ΔH_f : standard enthalpy of formation for the ideal gas at 298.2K

The reference states chosen for the elements are as follows:

Ideal gases at one atmosphere: Ar, Cl₂, D₂, F₂, He, H₂, Kr, Ne, O₂, Rn, T₂, and Xe.

Al (crystal); As (crystal); B (crystal); Br₂ (liquid); C (graphite); Hg (liquid); I₂

(crystal); P (solid, red); S (crystal. rhombic); Se (crystal); Si (crystal); Ti (crystal,

alpha); U (crystal).

** C₄H₆ here is 1,3-butadiene

*** the physical properties of n-C₅H₁₂ is used for C₅⁺

2. Component heat capacity constants

Isobaric heat capacity for ideal gas:

$$C_p = C_{pA} + C_{pB} \cdot T + C_{pC} \cdot T^2 + C_{pD} \cdot T^3$$

where

C_p : heat capacity $J/mole \cdot K$

T : temperature K

$C_{pA}, C_{pB}, C_{pC}, C_{pD}$: heat capacity constants listed in the following table.

Table E.2. Heat capacity constants for molecular species.

No.	Component	C _{pA}	C _{pB}	C _{pC}	C _{pD}
1	H ₂	2.714×10	9.274×10 ⁻³	-1.381×10 ⁻⁵	7.645×10 ⁻⁹
2	CH ₄	1.925×10	5.213×10 ⁻²	1.197×10 ⁻⁵	-1.132×10 ⁻⁸
3	C ₂ H ₂	2.682×10	7.578×10 ⁻²	-5.007×10 ⁻⁵	1.412×10 ⁻⁸
4	C ₂ H ₄	3.806	1.566×10 ⁻¹	-8.348×10 ⁻⁵	1.755×10 ⁻⁸
5	C ₂ H ₆	5.409	1.781×10 ⁻¹	-6.938×10 ⁻⁵	8.713×10 ⁻⁹
6	C ₃ H ₆	3.710	2.345×10 ⁻¹	-1.160×10 ⁻⁴	2.205×10 ⁻⁸
7	C ₃ H ₈	-4.224	3.063×10 ⁻¹	-1.586×10 ⁻⁴	3.215×10 ⁻⁸
8	C ₄ H ₆	-1.687×10	3.419×10 ⁻¹	-2.340×10 ⁻⁴	6.335×10 ⁻⁸
9	1-C ₄ H ₈	-2.994	3.532×10 ⁻¹	-1.990×10 ⁻⁴	4.463×10 ⁻⁸
10	n-C ₄ H ₁₀	9.487	3.313×10 ⁻¹	-1.108×10 ⁻⁴	-2.822×10 ⁻⁹
11	C ₅ ⁺	-3.626	4.873×10 ⁻¹	-2.580×10 ⁻⁴	5.305×10 ⁻⁸
23	H ₂ O	3.194×10	1.436×10 ⁻³	2.432×10 ⁻⁵	-1.176×10 ⁻⁸

3. Free radical heat capacity*

$$\text{Heat capacity for the free radical: } C_p = \frac{C_{p(300)} + C_{p(800)}}{2}$$

where

C_p : heat capacity $J/mole \cdot K$

$C_{p(300)}$: heat capacity at $T = 300K$

$C_{p(800)}$: heat capacity at $T = 800K$.

Table E.3. Heat capacity for free radicals.

No.	Free radical	$C_{p(300)} (J/mole \cdot K)$	$C_{p(800)} (J/mole \cdot K)$
12	H•	20.9	20.9
13	CH ₃ •	36.8	48.2
14	C ₂ H ₃ •	40.6	N/A
15	C ₂ H ₅ •	46.5	95.4
16	C ₃ H ₅ •	63.6	94.2**
17	1-C ₃ H ₇ •	71.5	141.0
18	2-C ₃ H ₇ •	73.3	138.8
19	C ₄ H ₇ •	87.0	130.2**
20	1-C ₄ H ₉ •	97.1	190.9
21	2-C ₄ H ₉ •	96.2	190.0
22	C ₅ H ₁₁ •	118.9	N/A

* *Handbook of Chemistry and Physics*, 54th edition, 1973-1974

**This heat capacity is measured at $T = 500K$

4. State-equation parameters for components

Table E.4. State-equation parameters for components.

No.	Component	T _c (K)	P _c (Bar)	ω	T _b (K)	Dipm(debye)	Z _c
1	H ₂	33.0	12.9	-0.216	20.3	0.0	0.303
2	CH ₄	190.4	46.0	0.011	111.6	0.0	0.288
3	C ₂ H ₂	308.3	61.4	0.190	188.4	0.0	0.270
4	C ₂ H ₄	282.4	50.4	0.089	169.3	0.0	0.280
5	C ₂ H ₆	305.4	48.8	0.099	184.6	0.0	0.285
6	C ₃ H ₆	364.9	46.0	0.144	225.5	0.4	0.274
7	C ₃ H ₈	369.8	42.5	0.153	231.1	0.0	0.281
8	C ₄ H ₆	425.0	43.3	0.195	268.7	0.0	0.270
9	1-C ₄ H ₈	419.6	40.2	0.191	266.9	0.191	0.277
10	n-C ₄ H ₁₀	425.2	38.0	0.199	272.7	0.199	0.274
11	C ₅ ⁺	469.7	33.7	0.251	309.2	0.1	0.263

PERMISSION TO COPY

In presenting this thesis in partial fulfillment of the requirements for a master's degree at Texas Tech University or Texas Tech University Health Sciences Center, I agree that the Library and my major department shall make it freely available for research purposes. Permission to copy this thesis for scholarly purposes may be granted by the Director of the Library or my major professor. It is understood that any copying or publication of this thesis for financial gain shall not be allowed without my further written permission and that any user may be liable for copyright infringement.

Agree (Permission is granted.)

Student's Signature

Date

Disagree (Permission is not granted.)

Student's Signature

Date